

The value of C_5^0 for charge exchange scattering has a peak of 0.60 ± 0.15 mb. This is consistent with the peak above the background in C_5^- of about 1.5 mb observed in this experiment, if both amplitudes have $T = \frac{1}{2}$.

Finally it is interesting to note that the behavior of C_5^- is readily explained as a consequence of interference between the real part of a $J = \frac{5}{2}, I = \frac{1}{2}$ resonant amplitude for $N^*(1688)$ and the real part of a $J = \frac{7}{2}, I = \frac{3}{2}$ amplitude describing the $N^*(1928)$, provided that these have the same parity.

A more detailed discussion of the interpretation of the results of this experiment will be given in a paper (to be published) describing polarization measurements in the same momentum range.

VIII. CONCLUSIONS

$N^*(1688)$ has $I = \frac{1}{2}, J = \frac{5}{2}$; $N^*(1928)$ has $I = \frac{3}{2}, J = \frac{7}{2}$. The two resonances probably have the same parity.

ACKNOWLEDGMENTS

We are grateful for the friendly cooperation of the Nimrod operating crew and of the High-Energy Physics Engineering Group. Their assistance, particularly in the early days of operation of Nimrod, was a major contribution to the successful completion of the experiment. We are also grateful to P. J. Coleman, C. R. Cox, N. A. Cumming, R. Downton, K. S. Heard, R. Mackenzie, Miss J. Robertson, D. C. Salter, and D. C. Thomas for invaluable assistance in setting up the experiment and taking data.

Pion-Pion Interactions in π^-p Reactions at 2.1 BeV/c*

E. WEST,† J. H. BOYD, A. R. ERWIN, AND W. D. WALKER

University of Wisconsin, Madison, Wisconsin

(Received 28 April 1966)

An analysis is given of the interactions of two pions as they result from the reactions of negative pions incident upon protons with a momentum of 2.1 BeV/c. A historical background of the motivation for the experiment is given and experimental techniques for dealing with the data are described, from the points of view of both event-by-event analysis and the physical theories which aid in the understanding of the results. Cross sections are given for the various reactions and are inferred by Chew-Low methods for pion-pion scattering. Evidence is presented which indicates that two resonant states in addition to the ρ meson and $N_{3/2}^*(1238)$ are present in these reactions: (1) the $N_{3/2}^*(1920)$, whose existence in other reactions is well established, and (2) the $T=0, s$ -wave pion-pion interaction, which is still in doubt, known as the e^0 , the evidence for which stems from an analysis of the decay distribution of the ρ^0 . Finally, corrections to the one-pion-exchange model which involve pion-nucleon scattering vertices are made in an attempt to determine more accurately the low-energy, $T=0, s$ -wave pion-pion scattering cross sections, the results suggesting a range of about 10-15 mb in the region below the ρ .

I. INTRODUCTION

THE development of bubble chambers, and especially of liquid-hydrogen bubble chambers, has allowed the accumulation of a vast body of empirical data involving inelastic interactions between fundamental particles.

Many of the properties of these resonances are well measured and in several cases accurate predictions were made on the basis of earlier data. For example, the earliest data on pion production in pion-nucleon collisions indicated that above an energy of 1 BeV a small momentum transfer to the nucleon is preferred.¹ This observation has led directly to our present recognition that the one-pion-exchange (OPE) interaction is an

important part of the over-all process. Physically this can be imagined as an incident pion striking a target furnished in a virtual state by the nucleon.

Analysis of electromagnetic data also implied that there must be a strong pion-pion interaction^{2,3} which, in fact, probably had the form of a resonance in the $T=1, J=1$ and $T=0, J=1$ states.³ In addition a π - P phase-shift analysis was used to deduce an energy for the resonance of about 660 MeV.⁴ Other data indicated a peak in the spectrum at an energy near 600 MeV.⁵

² W. Holladay, Phys. Rev. **101**, 1198 (1956).

³ W. R. Frazer and J. R. Fulco, Phys. Rev. Letters **2**, 365 (1959).

⁴ J. Bowcock, N. Cottingham, and D. Lurie, Phys. Rev. Letters **5**, 386 (1960); Nuovo Cimento **19**, 142 (1961). Also see J. A. Anderson, Vo X. Bang, P. G. Burke, D. D. Carmony, and N. Schmitz, Phys. Rev. Letters **6**, 365 (1961).

⁵ E. Pickup, F. Ayer, and E. O. Salant, Phys. Rev. Letters **5**, 161 (1960); in *Proceedings of the Tenth Annual International Conference on High Energy Physics at Rochester* (Interscience Publishers, Inc., New York, 1960); see also F. Bonsignori and F. Selleri, Nuovo Cimento **15**, 465 (1960).

* Work supported in part by the U. S. Atomic Energy Commission under contract No. AT(11-1)-881, COO-881-59.

† Now at the University of Toronto, Toronto, Ontario, Canada.

¹ L. M. Eisberg, W. B. Fowler, R. M. Lea, W. D. Shephard, R. P. Shutt, A. M. Thorndike, and W. L. Whittmore, Phys. Rev. **97**, 797 (1955); W. D. Walker and J. Crussard, *ibid.* **98**, 1416 (1955).

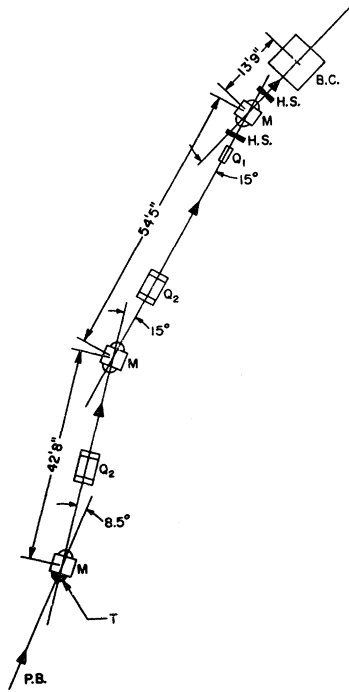


FIG. 1. Beam setup. B.C.—Bubble chamber; H.S.—Hevimet slit (2); M—H Magnet (3), 18 in. wide, 36 in. long; Q_1 —Quadrupole, 8 in. wide, 16 in. long; Q_2 —Quadrupole, 12 in. wide, 40 in. long; T—Target; P.B.—Proton beam from cosmotron. Shielding not shown. Not to scale.

All this evidence was tied together finally in 1961 when the ρ meson, as it was subsequently named, was directly observed by Erwin, March, Walker, and West⁶ as a correlation in the invariant mass of the two final-state pions from the reactions

$$\pi^- p \rightarrow \left\{ \begin{array}{l} \pi^- \pi^0 p \\ \pi^- \pi^+ n \end{array} \right\},$$

with an incident pion momentum of 1.89 BeV/c. This correlation takes the form of a large, broad peak in the distribution of the invariant mass near 760 MeV with a width of approximately 130 MeV.

The broad width of the ρ implies that it is a strongly decaying particle and thus the interaction conserves

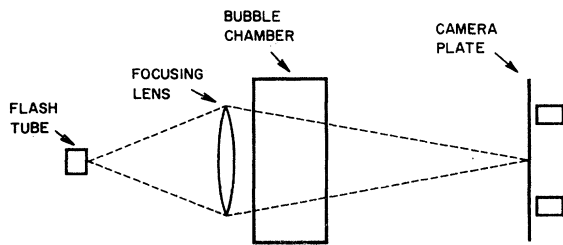


FIG. 2. Schematic diagram of flash tube, chamber, lens, and camera orientation.

⁶ A. R. Erwin, R. March, W. D. Walker, and E. West, Phys. Rev. Letters 6, 628 (1961).

such quantities as parity, G parity, spin (J), and isospin (T). These properties of the resonance were determined rather simply. The ρ is a resonant particle with

- (1) positive G parity since it decays into two pions;
- (2) $T=1$ by virtue of its measured branching ratio into different charge states;
- (3) $J=1$ since the spin must be odd according to Bose statistics for two pions in an odd isospin state and since the decay angular distribution for the ρ has the form $\cos^2\theta$;
- (4) negative parity since $P=(-1)^J$ for two pions and J is odd.

In addition, it was clear that the production mechanism for the ρ was strongly dominated by an interaction in which small momentum transfers to the nucleon were preferred.

A definitive study of the ρ with the 1.89-BeV/c experiment was not feasible, however, owing to both a lack of sufficient numbers of events and a rather poorly defined beam which made precision analysis very difficult. Thus a new proposal was offered and accepted to study the ρ meson, its production mechanism, and other competing interactions with a well-defined negative pion beam of 2.10 BeV/c.

II. EXPERIMENTAL METHODS

A. Beam

The system of magnets used at the Cosmotron which provided the necessary focusing and momentum analysis is shown schematically in Fig. 1. This arrangement was designed to produce a beam with a momentum of 2.1 BeV/c and a resolution of about 2%. Subsequently wire tests and direct measurements of beam tracks on film verified that the beam momentum actually was 2.1 BeV/c.

An additional check on this determination was possible from measurements made of events known to have a Λ^0 , K^0 final state in which both neutral particles are observed to decay. Since only angle measurements are used in this procedure (and not the less accurately known curvatures) a very precise value for the beam track momentum can be obtained by direct calculation. Eventually a mean beam momentum and width were obtained which verified the earlier determinations. From this point on, then, the beam momentum will be taken as 2.10 ± 0.04 BeV/c.

B. Bubble Chamber

The Adair-Leipuner 14-in. liquid-hydrogen bubble chamber was the final target in which 140 000 pictures were taken. Expansion of the chamber in synchronization with the beam produced trails of bubbles in the liquid which showed the path that each particle had taken as it traversed the liquid. These bubbles were recorded simultaneously by three cameras using a

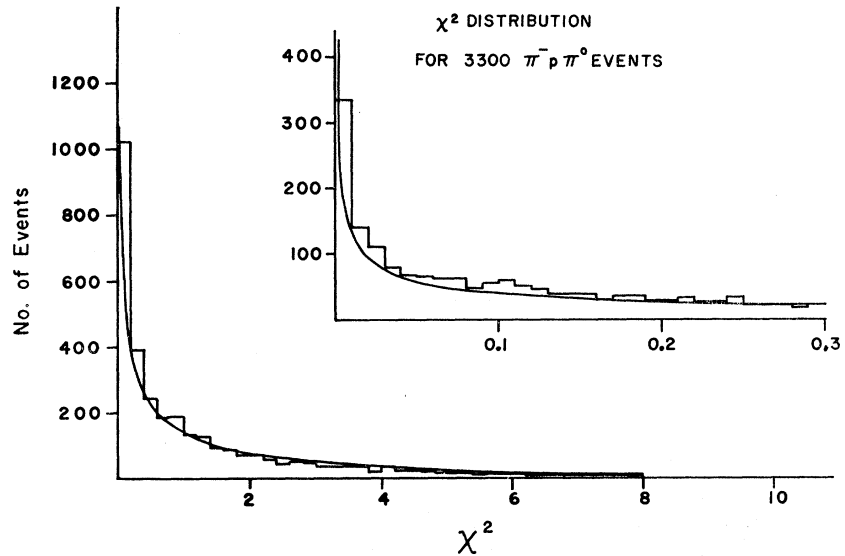


FIG. 3. χ^2 distribution for events assigned as $\pi^-p \rightarrow \pi^-p\pi^0$.

single flash tube for illumination with a system of dark field photography. The arrangement of flash tube chamber, focusing lens, and cameras is shown schematically in Fig. 2. The three cameras are placed outside the circle of direct illumination.

The magnetic field at the center of the chamber was 17.15 kG. Deviations of the field from this nominal value were small, but careful measurements had been made so that the true value of the axial field at any point inside the chamber was known, and calculations were made with full account taken of these deviations.

C. Scanning and Measuring

Events found within a selected fiducial volume were measured with the usual type of projection microscope. We required that beam tracks be at least 1.5 cm in length to permit an accurate determination of its direction. A forward going secondary track had a minimum visible length of 15 cm to permit its momentum to be well determined.

D. Computer Calculations

Computer programs were used which ideally should be able to determine exactly what type of event had been measured and to calculate for that event the relevant physical quantities. Because our measurements were not accurate enough to rely solely on computerized decisions, each event was subjected to a human analysis which took into account not only the computer output, but also certain nonmeasured characteristics of the event, including ionization estimates of the various tracks and a judgment of the reliability of measurement.

Four separate computer programs were used in the course of this experiment for use with an IBM 704 and a Control Data 1604.

The 704 spatial reconstruction program was written by A. R. Erwin and D. Lyon.⁷ The 1604 program, developed by R. W. Hartung, uses the fact that any point on the film is the projection of a ray running through the chamber. For every point measured on the film it is possible to construct a ray through the chamber which comes very close to intersecting the trajectory of the particle. Since the magnetic field is not far from uniform and most particles lose very little energy over their visible path length, the first approximation to this trajectory is a helix.

A least-squares fit is used to determine which helix is most accurately defined by the set of rays passing near it. In fact all the tracks which intersect at the same vertex are fitted simultaneously in such a way that the vertex also is determined without direct measurement. In addition this method affords a simple device for

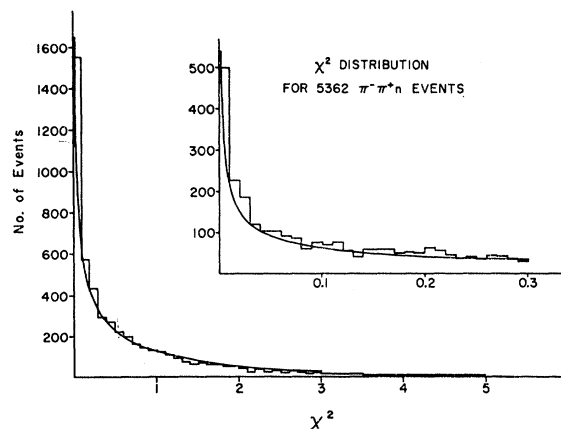


FIG. 4. χ^2 distribution for events assigned as $\pi^-p \rightarrow \pi^-\pi^+n$.

⁷ Paul H. Satterblom, doctoral thesis, University of Wisconsin, 1963 (unpublished).

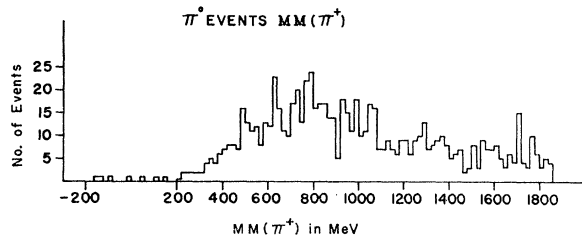


FIG. 5. Missing mass distribution of events assigned $\pi^-p\pi^0$ assuming p was π^+ .

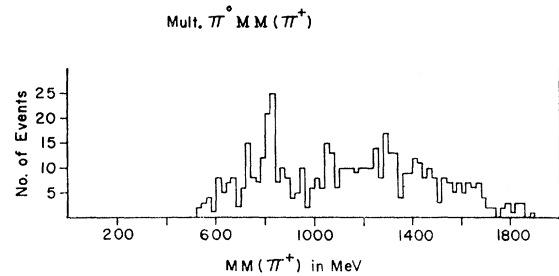


FIG. 7. Missing mass distribution of events assigned π^-pX assuming p was π^+ .

determining the accuracy of the measurement because the quantity being minimized in the least-squares fit is the sum of squares of the distances of the rays from the helix.

Kinematic fitting procedures for the two machines both used the usual χ^2 technique. The 704 version was based on the Berkeley GUTS subroutine⁸ as adapted by L. Leipuner and J. H. Boyd. For 1604 processing R. H. March's subroutine FIT performed the fitting process.

E. Event Identification

1. Event Assignments

Almost all events fall into one of the following classifications:

$$\pi^-p \rightarrow \pi^-p, \quad (1)$$

$$\rightarrow \pi^-p\pi^0, \quad (2)$$

$$\rightarrow \pi^-p\pi^+\pi^0, \quad (3)$$

$$\rightarrow \pi^-pX, \quad (X = \pi^0\pi^0 \dots), \quad (4)$$

$$\rightarrow \pi^-p\pi^+Y, \quad (Y = n\pi^0 \dots). \quad (5)$$

An analysis of the elastic events will be part of the thesis of J. H. Boyd.⁹

2. Internal Consistency

That our assignment procedure resulted in very nearly the correct distribution in χ^2 values (see Figs.

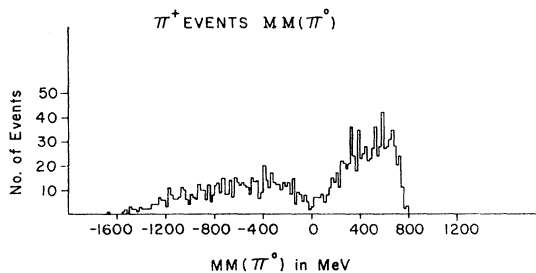


FIG. 6. Missing mass distribution of events assigned $\pi^-p\pi^+n$ assuming π^+ was p .

⁸ J. P. Berge, F. T. Schmitz, and H. D. Taft, Lawrence Radiation Laboratory Report UCRL-9097, 1960 (unpublished).

⁹ The thesis of J. H. Boyd will contain a discussion of elastic scattering as well as certain aspects of $\pi^-p\pi^+Y$ events, for example, a search for K^-K^+n and $\pi^-K^+\Lambda^0$ events where no decay is observed.

3 and 4) indicates that whatever systematic errors in assignments exist are probably very small. The graphs of the χ^2 distribution indicate only a slight excess of events in the small χ^2 region for which two explanations exist: (1) events for which no selection criteria exist except χ^2 are discriminated against if χ^2 is large, and (2) error assignments are slightly too large on the average. That the χ^2 distribution is approximately correct is evidence that the original measurement errors themselves are close to being correct.

Further evidence that event identifications were correctly made is provided by Figs. 5 through 8 which show the missing mass for the "wrong" assignments; for example, if an event was assigned a π^-pX final state, Fig. 7 shows the neutral mass assuming the positive track was a pion. If there were a systematic tendency to assign, say a $\pi^-p\pi^+Y$ final state as $\pi^-p\pi^0$, Fig. 5 would show a broad enhancement for mass values above 1075 MeV which it does not. All the evidence from this analysis indicates that our event identification was very accurate.

The neutral mass distributions for the assignments actually made are shown in Figs. 9 and 10. Both graphs show superimposed the single and multiple production events. Events in the overlap region were separated on the basis of the χ^2 value.

3. Contaminations and Biases

Probably the most perplexing difficulties in event assignments arose in the analysis of events with a particular topology which could be either elastic or $\pi^-p\pi^0$. These events had a proton and a π^- with equal laboratory scattering angles (and for elastic events therefore the same momentum). The accuracy of our measurements was simply not good enough to prove or disprove the existence of a π^0 which in the center-of-momentum system would be at rest. Often both interpretations have low χ^2 values, but with no other method available this problem was resolved in favor of the χ^2 value with the highest probability. This problem was rare and should not cause difficulty in any later analysis.

No other assignment errors are thought to be significant or in any way to affect the results to be presented.

Also it should be noted that large numbers of small-angle scattering elastic events are missed in scanning. These events in the diffraction peak have a very short stopping proton and the pion undergoes only a very small scatter. An extrapolation estimate of the number of these events missed will form part of Boyd's thesis.⁹ For now let it be noted that these events are taken into account in the cross-section calculations discussed in Sec. IV.

III. THEORETICAL MODELS

Although theoretical physicists have failed to produce an all-encompassing theory to explain the various phenomena which are characteristic of strong interactions, certain specific models have led to a limited understanding of the processes involved. Our results are discussed in terms of these models which are briefly discussed here.

A. Statistical

The statistical model of strong interactions is really only a mathematical construct which hypothesizes that in fact there are no interactions in the final state; that is, that the probability that a particle exists in a given state is proportional to the invariant four-dimensional phase-space volume d^4P . This is identical to letting the square of the covariant matrix element T be a constant.

The important result of this model is that the kinematically accessible region of a Dalitz plot is uniformly populated. A deviation from uniformity in the experimentally determined Dalitz plot is definite evidence that $|T|^2 \neq \text{const}$ and that an energy- or angle-dependent interaction between the particles is important.

B. One-Pion Exchange

The physical picture of the incident pion striking a pion in the mesonic cloud of the nucleon suggests that for some events the nucleon plays a minor role in the final state, its part in the interaction being limited to the emission of the target pion.

The physical variable which is used as a measure of the degree of nucleon participation in the interaction is the square of the invariant momentum transfer, defined by

$$t = (E_f - E_i)^2 - (\mathbf{P}_f - \mathbf{P}_i)^2. \quad (6)$$

In this formula the variables refer to the initial and final

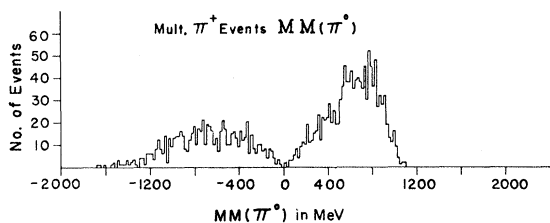


FIG. 8. Missing mass distribution of events assigned $\pi^-\pi^+Y$ assuming π^+ was p .

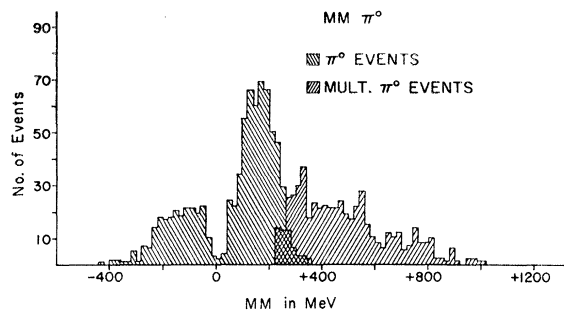


FIG. 9. True neutral mass distribution for events assigned $\pi^-p\pi^0$ and π^-pX .

four-momenta of the nucleon. For physically possible processes t is negative; therefore we also define

$$\Delta^2 = -t. \quad (7)$$

A small value of Δ corresponds to minimal nucleon participation.

1. Chew-Low Extrapolation

The fundamental assumption of the physical model outlined above is that only the one-pion-exchange (OPE) diagram [shown in Fig. 11(a)] is important in the interaction. One consequence is the following formula which relates pion-pion scattering to the total pion production process:

$$\left(\frac{\partial^2 \sigma}{\partial t \partial \omega^2}\right)_{\text{CL}} \xrightarrow{t \rightarrow \mu^2} \alpha \left(\frac{f^2}{2\pi}\right) \frac{-t/\mu^2}{(t-\mu^2)^2} \times \frac{\omega [(\omega^2/4) - \mu^2]^{1/2}}{\bar{K}_L^2} \sigma_{\pi\pi}(\omega). \quad (8)$$

Here ω is the invariant mass of the two pions (each of mass μ), \bar{K}_L is the incident pion momentum measured in the laboratory, $f^2 = 0.08$ is the $pp\pi^0$ coupling constant, and $\alpha = 1$ or 2 for $\pi^-p\pi^0$ or $\pi^-\pi^+n$ final states, respectively.

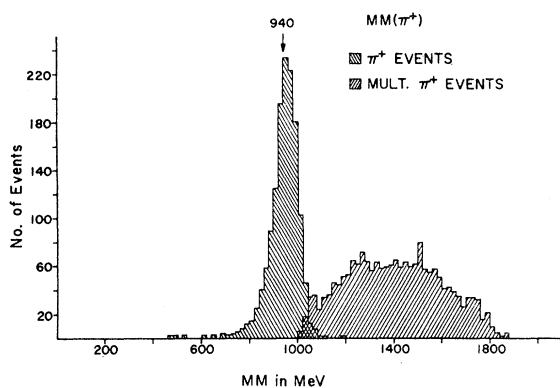
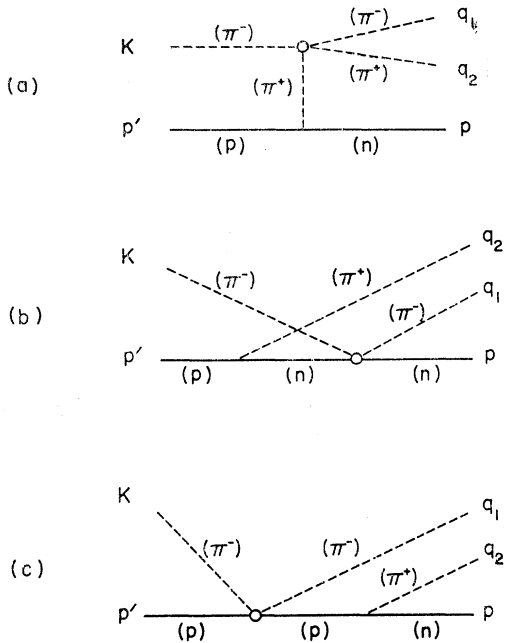


FIG. 10. True neutral mass distribution for events assigned $\pi^-\pi^+n$ and $\pi^-\pi^+Y$.

FIG. 11. Lowest order Feynman diagrams for $\pi^- p \rightarrow \pi^- \pi^+ n$.

The above formula, originally derived by Goebel,¹⁰ was put in this form by Chew and Low¹¹ for whom it is now named. Chew and Low further suggested how it may be used to obtain a knowledge of the pion-pion cross section by extrapolating measured data from the physical region to the unphysical pole at $t = \mu^2$. We define the function

$$f(t, \omega) = \frac{2\pi \bar{K}_L^2}{\alpha f^2} \frac{(t - \mu^2)^2}{\omega [(\omega^2/4) - \mu^2]^{1/2}} \left(\frac{\partial^2 \sigma}{\partial t \partial \omega^2} \right)_{CL}, \quad (9)$$

which can be calculated from the experimental data for each small region defined by a particular choice of t and ω . The Chew-Low formula then implies that

$$\lim_{t \rightarrow \mu^2} f(t, \omega) = -\sigma_{\pi\pi}(\omega). \quad (10)$$

An alternative use of the Chew-Low formula is to assume that the OPE pole term dominates even some distance away from the pole so that the formula is valid also in the physical region. Integration of (8) over the useful range of t then yields directly an equation for $\sigma_{\pi\pi}(\omega)$.

The degree to which low momentum transfer events dominate a particular interaction can be displayed graphically by means of a Chew-Low plot, a scatter diagram where each event is represented by a point whose coordinates are t and ω^2 . The OPE model predicts a dense clustering of points in the region of small t .

¹⁰ C. Goebel, Phys. Rev. Letters **1**, 337 (1958).

¹¹ G. F. Chew and F. E. Low, Phys. Rev. **113**, 1640 (1959).

2. Treiman-Yang Test

It was pointed out by Treiman and Yang¹² that any interaction which proceeds through the exchange of a single spinless particle (such as a pion) must have an interaction rate which is invariant with respect to rotations about the axis defined by the momentum of the exchanged particle. The experimental test is to determine the distribution of the angle between the plane of production of the dipion and the plane of its decay; that is, the distribution of ϕ_{TY} , where

$$\cos \phi_{TY} = \frac{\mathbf{P} \times \mathbf{P}_1 \cdot \mathbf{q}_1 \times \mathbf{q}_2}{|\mathbf{P} \times \mathbf{P}_1| |\mathbf{q}_1 \times \mathbf{q}_2|} \quad (11)$$

[the definition of these quantities is shown in Fig. 11(a)], as computed, say, in the coordinate system in which the incident pion is at rest. Note that this definition may differ by a sign from that used in other experiments.

C. OPE with Selleri Corrections

The Chew-Low formula has been modified by Selleri¹³ to take into account two effects: (1) the off-the-mass-shell character of the π - π interaction, and (2) possible form factors for the pion-dipion vertices and the pion propagator. The Selleri formula is related to the original Chew-Low formula by

$$\left(\frac{\partial^2 \sigma}{\partial t \partial \omega^2} \right)_S = \left[\left(\frac{q'}{q} \right)^l F(t) \right]^2 \left(\frac{\partial^2 \sigma}{\partial t \partial \omega^2} \right)_{CL}, \quad (12)$$

where l refers to the dominant spin state of the π - π interaction at total energy w . The form factor $F(t)$ is given by Selleri^{13,14} as

$$F(t) = \frac{3.41}{5.73 - (t/\mu^2)} + 0.28 \quad (13)$$

and

$$q'^2 = (1/4\omega^2)[(\omega^2 - t + \mu^2)^2 - 4\omega^2\mu^2],$$

$$q^2 = \omega^2/4 - \mu^2.$$

This semi-empirical form factor results from an analysis of $N_{3/2}^*(1238)$ production in nucleon-nucleon collision in terms of OPE.¹⁴ Selleri suggests that the region of good approximation of this formula is $-t < 10\mu^2$.

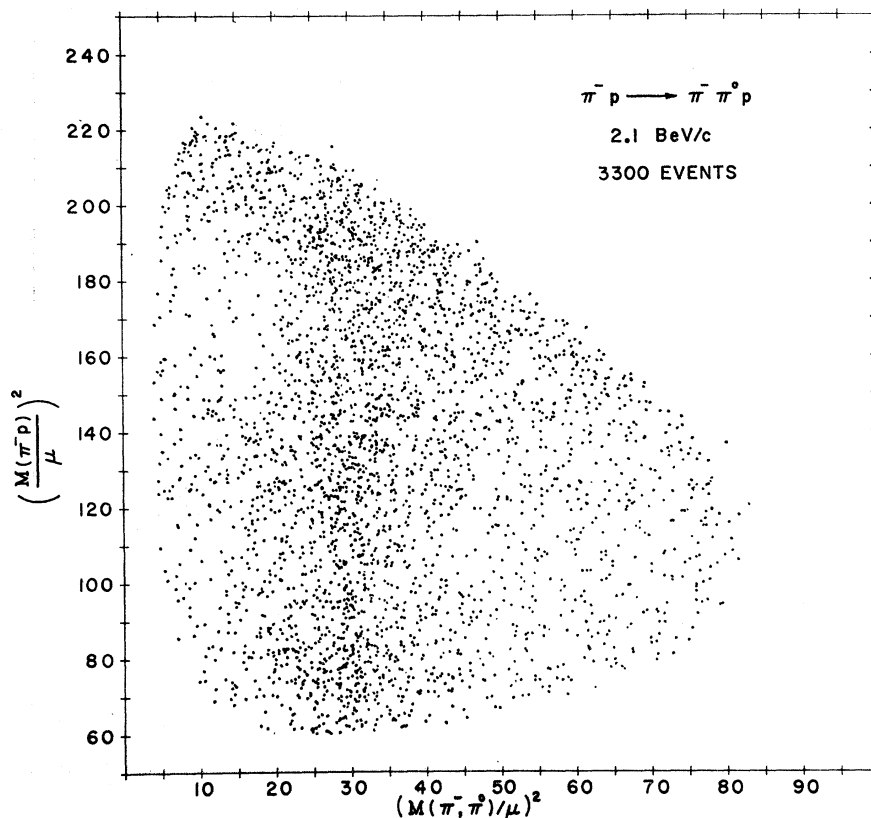
D. OPE with Absorption

It is known that ρ -production angular distributions are more peaked in the forward direction than is predicted by the OPE model. The invocation of form

¹² S. B. Treiman and C. N. Yang, Phys. Rev. Letters **8**, 140 (1962).

¹³ F. Selleri, Phys. Letters **3**, 76 (1962).

¹⁴ E. Ferrari and F. Selleri, Nuovo Cimento **23**, 1450 (1963); Phys. Rev. Letters **7**, 387 (1961).

FIG. 12. Dalitz plot for $\pi^-p\pi^0$.

factors to account for these results implies the existence of light particles which have not been observed.

To avoid curve-fitting devices of this type several authors^{15,16} have recently attempted to modify OPE in a more fundamental way by taking into account the many competing channels which together make a large contribution to the total inelastic cross section. Also considered are the requirements of unitarity which are violated by OPE. One might expect the more complex final states to be produced in essentially head-on collisions, thus by unitarity, reducing the lowest partial wave amplitudes below those given by the simple OPE model.

The main consequences of this coupling to other channels are (a) a reduction in the reaction cross section, (b) a collimation of the production angular distribution, and (c) the creation of correlations in the decay of the unstable particle (in our case, the ρ). A sharpening of the production angular distribution of the ρ , of course, corresponds exactly to a peaking in the momentum-transfer distribution.

Gottfried and Jackson give the decay angular dis-

tribution²¹ as

$$W(\theta, \phi) = (3/4\pi)(\rho_{00} \cos^2\theta + \rho_{11} \sin^2\theta - \rho_{1,-1} \sin^2\theta \cos 2\phi - \sqrt{2} \operatorname{Re}\rho_{10} \sin 2\theta \cos\phi), \quad (14)$$

where the quantities $\rho_{mm'}$ are the elements of the vector meson's spin-space density matrix and the angles are the same as have been defined above (θ , the π - π scattering angle; ϕ , the Treiman-Yang angle). Note also that ρ_{00} , ρ_{11} , and $\rho_{1,-1}$ are real. Each of the elements in the density matrix except $\operatorname{Im}\rho_{10}$ may be determined from experiment. Also the condition of a unit trace yields

$$\rho_{00} + 2\rho_{11} = 1. \quad (15)$$

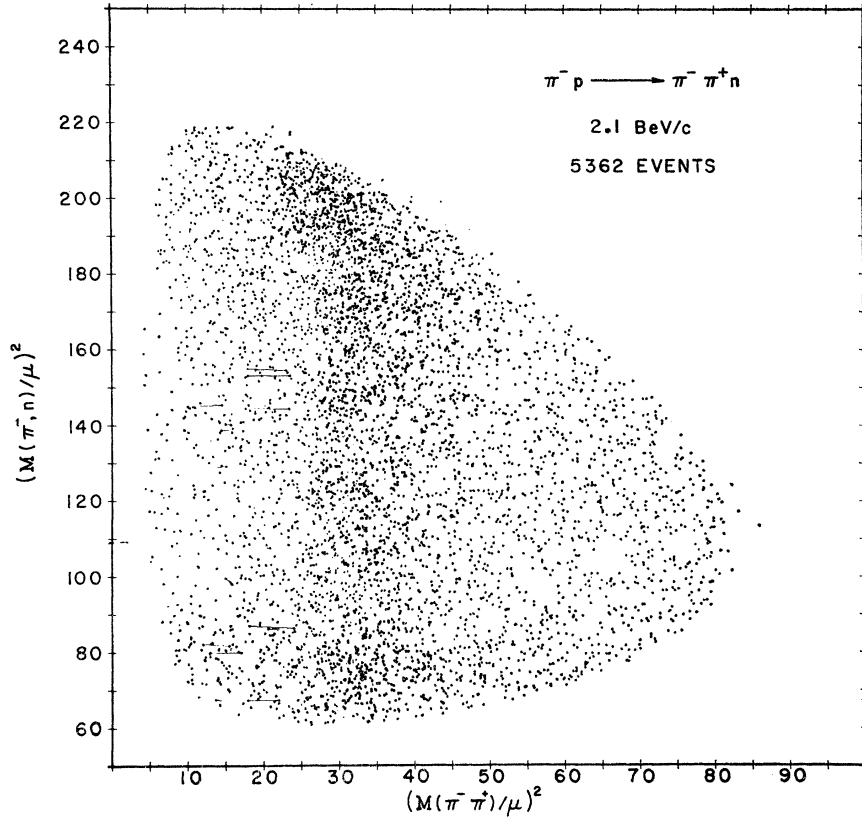
It is worth noting the following interesting facts about this model: (1) absorption processes change the density matrix elements from their OPE values so that ρ_{00} is no longer the only nonzero element, (2) the Treiman-Yang angular distribution may not be uniform since

$$I(\phi) = \int_{-1}^{+1} W d(\cos\theta) = \frac{1}{2\pi}(1 - 2\rho_{1,-1} \cos 2\phi) \quad (16)$$

and, (3) the π - π angular distribution may have an

¹⁵ K. Gottfried and J. D. Jackson, *Nuovo Cimento* **34**, 735 (1964); see also K. Gottfried and J. D. Jackson, *ibid.* **33**, 309 (1964).

¹⁶ L. Durand, III, and Y. T. Chiu, *Phys. Rev. Letters* **12**, 399 (1964); **13**, 45(E) (1964); *Phys. Rev.* **137**, B1530 (1965); *Phys. Rev. Letters* **14**, 329 (1965); **14**, 680(E) (1965).

FIG. 13. Dalitz plot for $\pi^- \pi^+ n$.

isotropic component since

$$I(\theta) = \int_0^{2\pi} W d\phi = \frac{3}{2} [\rho_{11} + (1 - 3\rho_{11}) \cos^2 \theta] \quad (17)$$

using the trace condition.

It has been suggested that in addition to the ρ a $T=0$, s -wave resonance at nearly the ρ mass may also be produced. Such an object would interfere with the ρ and the decay angular distribution would then have the form²³

$$W(\theta, \phi) = (3/4\pi) [\langle a_0 a_0 \rangle \cos^2 \theta + \langle a_1 a_1 \rangle \sin^2 \theta - \sqrt{2} \langle a_1 a_0 \rangle \sin 2\theta \cos \phi - \langle a_1 a_{-1} \rangle \sin^2 \theta \cos 2\phi] + (\sqrt{3}/4\pi) [-2\sqrt{2} \langle a_1 b_0 \rangle \sin \theta \cos \phi + 2 \langle a_0 b_0 \rangle \cos \theta] + (1/4\pi) \langle b_0 b_0 \rangle, \quad (18)$$

where the quantities $\langle a_i a_j \rangle$, $\langle a_i b_j \rangle$, and $\langle b_0 b_0 \rangle$ are the density matrix elements appropriate to this situation. The trace condition becomes

$$\langle a_0 a_0 \rangle + 2 \langle a_1 a_1 \rangle + \langle b_0 b_0 \rangle = 1. \quad (19)$$

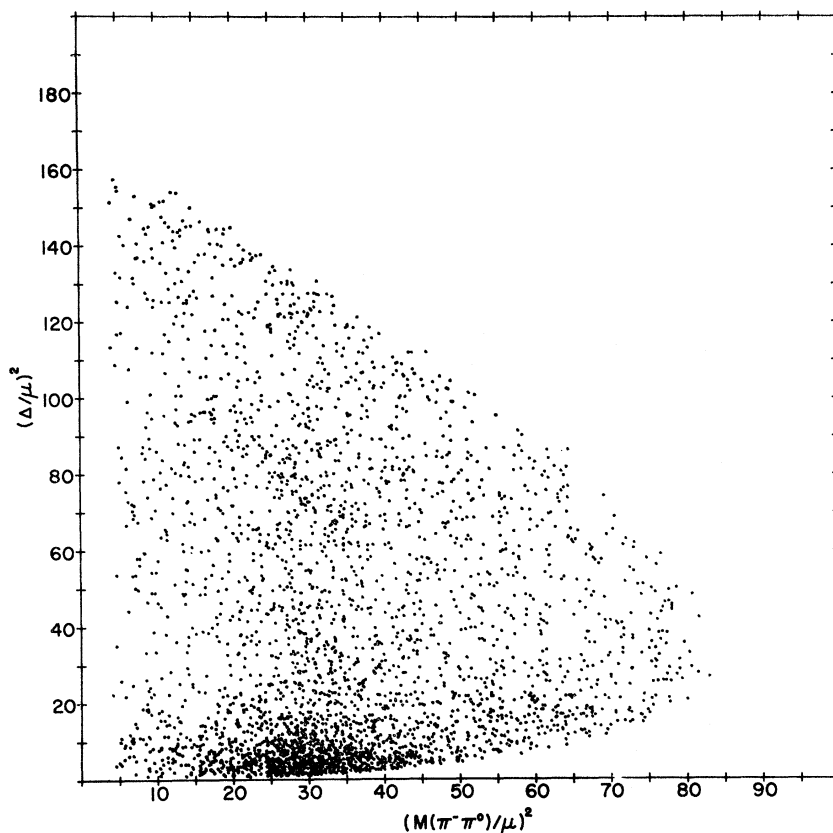
It should also be noted that since there are two contributions to an isotropic component, W is actually a function only of the difference $\langle a_1 a_1 \rangle - \langle a_0 a_0 \rangle$ (when the trace condition is taken into account). This means that fitting the experimental data does not uniquely determine the elements $\langle a_0 a_0 \rangle$, $\langle a_1 a_1 \rangle$, $\langle b_0 b_0 \rangle$, and additional information must be used.

E. OPE with Nucleon Corrections

The experimental data suggest that, although production via the one-pion-exchange mechanism is the single most important process involved, $\pi^- p$ interactions are not adequately described by a pure OPE model even including absorptive effects; contributions from other diagrams are significant, especially for the $\pi^- \pi^+ n$ final state. It may be that the most important non-OPE diagrams are those with poles closest to the physical region. To estimate the effect of taking these diagrams into account, we have made a rough field theoretic calculation of the $\pi^- \pi^+ n$ cross sections which includes all three of the diagrams shown in Fig. 11. It is hoped that this model will aid in particular the analysis of s -wave pion-pion scattering.

The full derivation of the cross section which results is given in Appendix A. Here we will merely list the important approximations which were used:

- (a) We did not include any absorptive effects.
- (b) Each scattering vertex is treated as if it were on the mass shell so that physical scattering amplitudes could be used.
- (c) The $T=1$ pion-pion interaction is given by a p -wave Breit-Wigner amplitude.¹³
- (d) The pion-nucleon interaction is given by pure diffraction scattering with suppression of the nonrelativistic anti-nucleon intermediate state. The ampli-

FIG. 14. Chew-Low plot for $\pi^-p\pi^0$.

tudes are obtained from the measured cross sections together with the optical theorem and a forward dispersion relation calculation.^{17,18}

The cross section is finally obtained as a function of ω , t , $\cos\theta_{\pi^-\pi^+}$, and $\phi_{\pi^+\pi^0}$. Since no absorption effects have been taken into account we expect the predicted cross sections to be larger than the true values. This turns out to be the case by about a factor of two. A further assumption then is that inclusion of absorptive effects will not significantly change the shape of any distribution other than momentum transfer.

A discussion of the success of this model and its application to pion-pion s -wave scattering appears in Sec. V.

IV. RESULTS

A. Cross Sections

The simplest results which are obtainable from our analysis are the cross sections for the various final states. These are listed in Table I. Our partial cross sections are normalized to a total cross section for scattering of 36.0 mb as obtained from the data of Diddens *et al.*¹⁹

¹⁷ J. W. Cronin, Phys. Rev. **118**, B82 (1960).

¹⁸ H. I. Saxer, doctoral thesis, University of Michigan, 1964 (unpublished).

¹⁹ A. N. Diddens *et al.*, Phys. Rev. Letters **10**, 262 (1963).

TABLE I. Partial cross sections for each of the two-prong final states including the correction for elastic scanning bias.

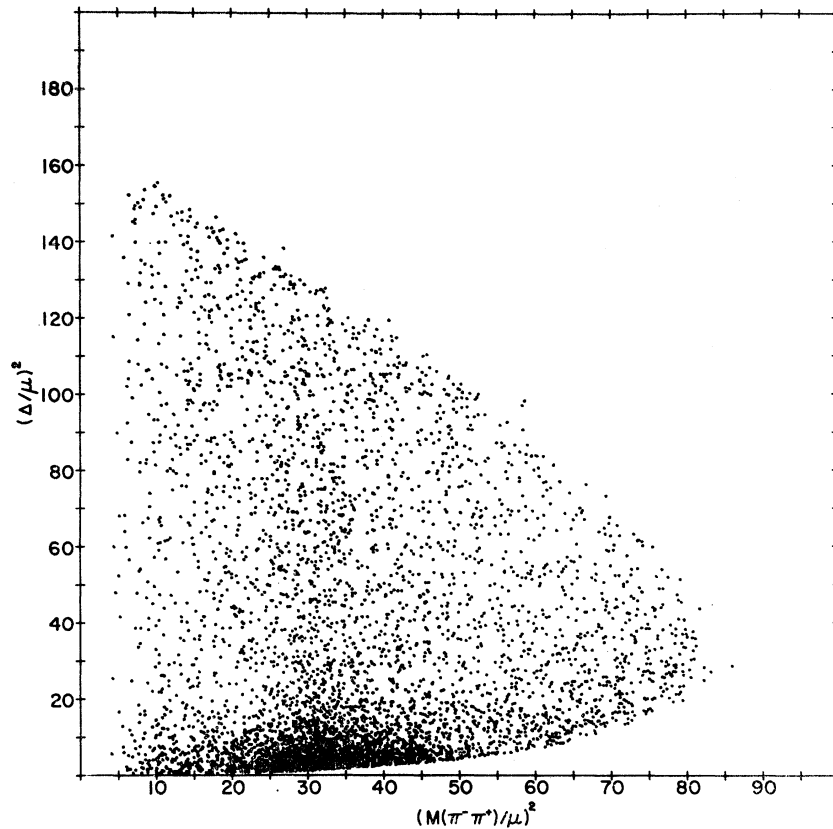
Reaction	Cross section in mb
(1) $\pi^-p \rightarrow \pi^-p$	9.69 ± 0.20
(2) $\pi^-p\pi^0$	3.33 ± 0.06
(3) $\pi^-\pi^+\pi^0$	5.67 ± 0.10
(4) π^-pX	1.93 ± 0.04
(5) $\pi^-\pi^+Y$	7.02 ± 0.13
(6) Non-two-prongs	8.35 ± 0.47

The division of the total cross section into two-prong and non-two-prong parts was done on the basis of a careful double scan of a systematically preselected set of frames by our best scanners. The subdivision into specific classifications was based on a larger group of events categorized as described in Sec. II. The number of events in each of these groups is listed in Table II.

In addition, a careful analysis of scanning bias for elastic events has been made by Boyd⁹ in order to correct for those small-angle elastic scatterings which are never found during scanning. This correction can be expressed as a ratio:

$$\frac{\text{Total number of elastic events}}{\text{Elastic events actually observed}} = 1.22 \pm 0.02.$$

Two simplifying assumptions were also made: (1)

FIG. 15. Chew-Low plot for $\pi^- \pi^+ n$.

the two-prong events which could not be assigned to any particular event type were distributed over the event types in the same way as those which were classified; and, (2) the data from the careful scan were independent of the total data, although in fact they were a subset of the total data.

The errors are Gaussian and are computed considering the correction factor and the number of events in each category as independent.

The analysis then makes use of the 8662 events which

TABLE II. The total numbers of events used for various analyses grouped according to final assignment or topology. Not all of the available inelastic two-pronged events were used for cross-section determinations. The number of elastic events does not include the scanning bias correction.

Type	Careful scan	Events used in cross-section analysis	Total useful inelastic events
$\pi^- p$ (uncorrected)		5050	
$\pi^- p \pi^0$		2123	3300
$\pi^- \pi^+ n$		3612	5362
$\pi^- p X$		1232	
$\pi^- \pi^+ Y$		4467	
Assigned two-prongs	512	16 484	
Unassigned two-prongs	302		
Total two-prongs	814		
Non-two-prongs	256		
Total events	1070		

finally were assigned to one or the other of the single-pion-production event types. For this group of events we have $1.08 \pm 0.02 \mu\text{b}$ per event.

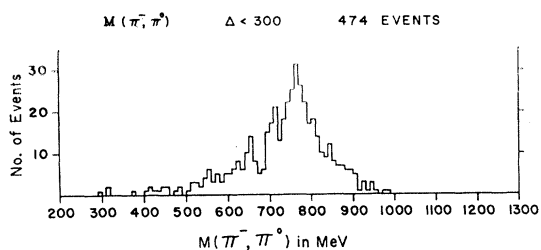
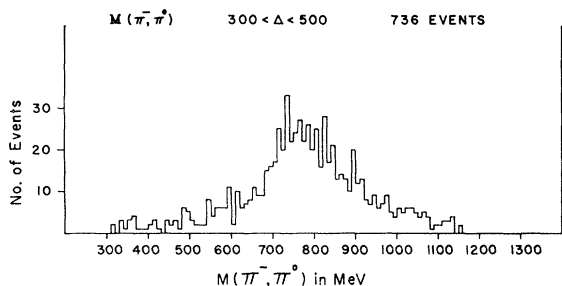
B. Final-State Interactions

1. Pion-Pion Reactions

Dalitz plots for the final states of this experiment are shown in Figs. 12 and 13. Both of these diagrams show clearly that the statistical model does not describe this interaction. The dominant characteristic of the diagrams is the increased density of points in the broad band centered near a pion-pion effective mass squared of $30\mu^2$ or a mass of about 760 MeV. This enhancement has come to be known as the ρ meson.

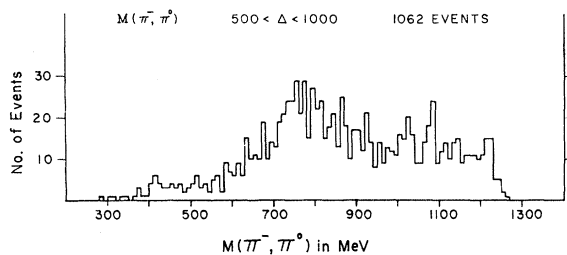
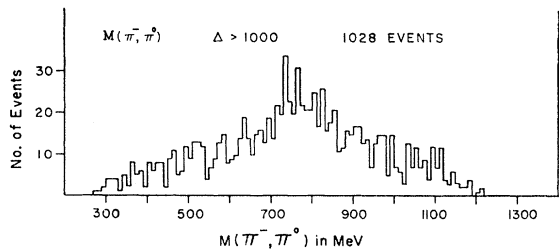
Chew-Low plots for these reactions are shown in Figs. 14 and 15. These diagrams make clear the strong enhancement in the region of low momentum transfer to the nucleon and for that particular class the dominance of the ρ . It is also clear from Figs. 12–15 that a substantial number of events have neither low momentum transfers nor a ρ .

Figures 16–23 show pion-pion mass distributions for various ranges of momentum transfer. The graphs for small Δ indicate clearly the broad enhancement corresponding to the ρ as well as the background of non- ρ events. The graphs for large Δ (as well as the Chew-Low

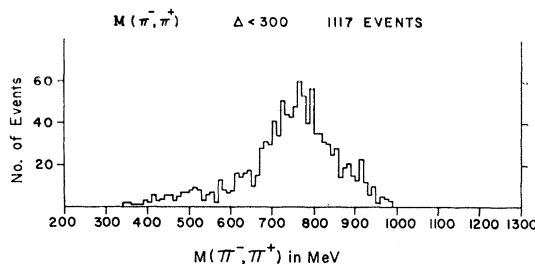
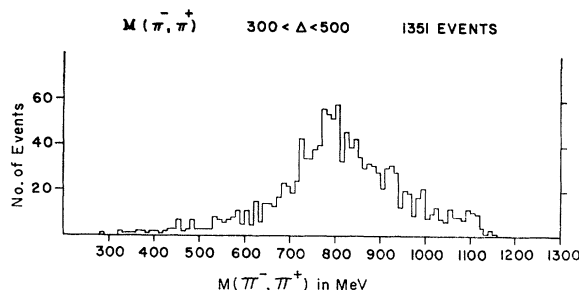
FIG. 16. Pion-pion mass distribution $M(\pi^-\pi^0)$ for $\Delta < 300$ MeV/c.FIG. 17. $M(\pi^-, \pi^0)$ for $300 \leq \Delta < 500$ MeV/c.

plots), however, show almost no enhancement near the ρ mass.

It should also be noted that none of these distributions by themselves indicate the existence of any additional pion-pion enhancements. Several fluctuations do appear but none are significant enough statistically to suggest the existence of a new resonance or to substantiate any of the previously suggested enhancements at low pion-pion masses.²⁰ The possibility of the use of

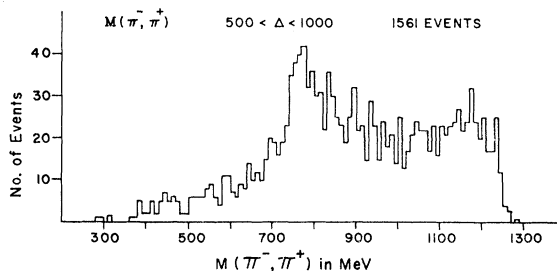
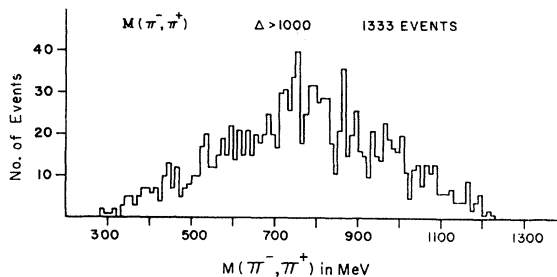
FIG. 18. $M(\pi^-, \pi^0)$ for $500 \leq \Delta < 1000$ MeV/c.FIG. 19. $M(\pi^-, \pi^0)$ for $\Delta \geq 1000$ MeV/c.

²⁰ For a complete tabulation of experiments relating to possible resonant states, see A. H. Rosenfeld *et al.*, Rev. Mod. Phys. **36**, 977 (1964); **37**, 633 (1965).

FIG. 20. $M(\pi^-, \pi^+)$ for $\Delta \leq 300$ MeV/c.FIG. 21. $M(\pi^-, \pi^+)$ for $300 \leq \Delta < 500$ MeV/c.

other data to infer the existence of any additional pion-pion interactions will be considered in Sec. VB3.

The distributions in momentum transfer for various ranges of $M(\pi\pi)$ as given in Figs. 24 and 25 indicate the peaking for small t/μ^2 . The effect occurs for all values of $M(\pi\pi)$ although an anomaly exists for $M(\pi^-\pi^0) < 0.400$ BeV (Fig. 24) in that a peak occurs at $-t = 10\mu^2$. This is most likely a statistical fluctuation since there are very few events in that region of the Chew-Low plot (Fig. 14).

FIG. 22. $M(\pi^-, \pi^+)$ for $500 \leq \Delta < 1000$ MeV/c.FIG. 23. $M(\pi^-, \pi^+)$ for $\Delta \geq 1000$ MeV/c.

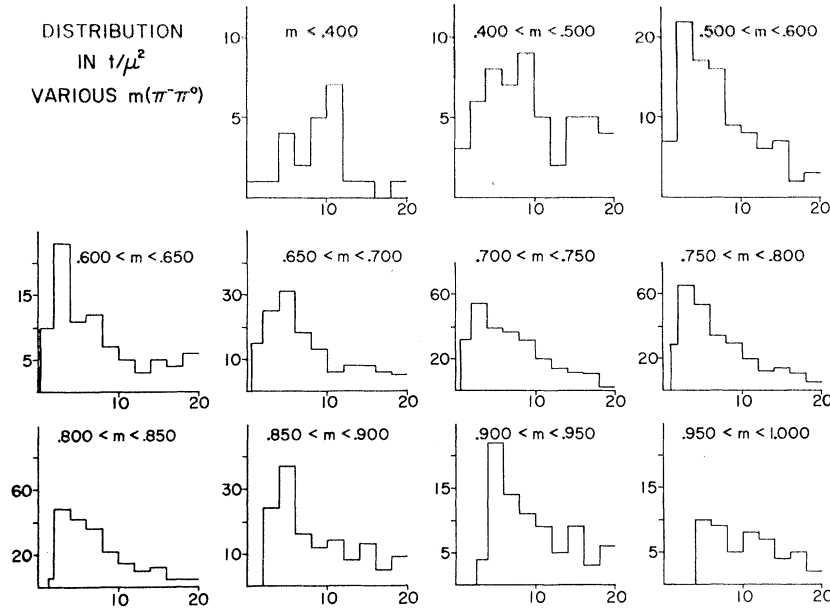


FIG. 24. Momentum transfer distributions $-t/\mu^2$ for various $M(\pi^-\pi^0)$.

Analysis of these distributions in terms of the Chew-Low formula or some variation of it allows us to infer some information concerning the pion-pion scattering process. This is discussed in Sec. V.

Figures 26-29 show the pion-pion scattering angular distribution. There are three points which should be noted:

(a) No significant differences seem to exist between the two range of t .

(b) In the mass range of the ρ the distribution has essentially a $\cos^2\theta$ shape, whereas for the lower mass values the distribution is more isotropic.

(c) The distributions of $\cos\theta(\pi^-\pi^+)$ show a strong forward peaking superimposed on the basic $\cos^2\theta$ shape.

Figures 30-33 show the Treiman-Yang angular distributions for various mass ranges and ranges of momentum transfer. There appears to be no large deviation from uniformity in these graphs.

However, if one plots a scatter diagram of ϕ_{TY} versus $\cos\theta(\pi\pi)$ it is seen that the two variables may not be independent. Figure 34 shows such a plot for 1225 events with $0.700 < M(\pi^-\pi^+) < 0.850$ BeV and $-t < 10\mu^2$. The enhancement of events for $\cos\theta \sim +1.0$, $\phi_{TY} \sim 180^\circ$ and to a lesser extent for $\cos\theta \sim -1.0$,

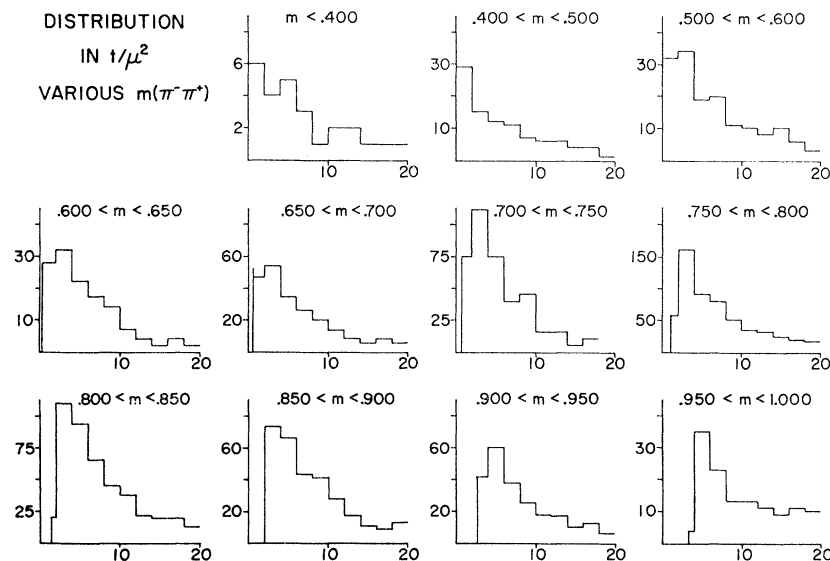


FIG. 25. $-t/\mu^2$ distribution for various $M(\pi^+\pi^+)$.

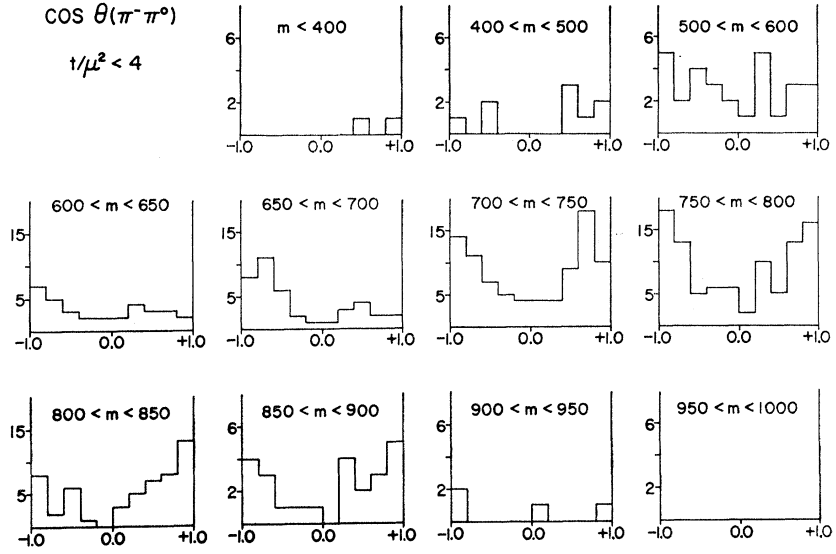


FIG. 26. Pion-pion center-of-momentum scattering angular distributions in $\cos\theta(\pi^-\pi^0)$, $-t/\mu^2 \leq 4$.

$\phi_{TY} \sim 0^\circ$ is obvious. This effect will be analyzed further in Sec. V. Also an analysis will be made of the same correlations for the 610 $\pi^-\pi^0$ events which meet these criteria. Note also that the sign of $\cos\phi_{TY}$ is reversed from that used in some experiments.

2. Pion-Nucleon Reactions

Although our main concern is with pion-pion reactions, it is relevant to discuss the final-state interactions of pions and nucleons. Figures 35-46 are the projections of the Dalitz plots (Figs. 12 and 13) on the axes representing the possible pion-nucleon combinations except that they have been subdivided into different groups depending on momentum transfer.

As the Dalitz plots indicate, the only significant feature to appear in this presentation of the data is the

large peak above 1700 MeV in the histogram of $M(\pi^-n)$, $\Delta < 500$ (Fig. 41) which is also reflected as a low-mass enhancement in the corresponding graph for π^+n (Fig. 44). This behavior may be in part due to the existence of the $T = \frac{3}{2}$ pion-nucleon resonance at 1920 MeV. But it is also connected kinematically with the pion-pion scattering process and in particular with the distribution in $\cos\theta(\pi^-\pi^+)$. This will be pursued further in Sec. V.

V. ANALYSIS

A. ρ Production

The Dalitz plots (Figs. 12 and 13) suggest that a fair approximation to the distribution of events would be a combination of resonance production and a uniform background, i.e., a statistical-model distribution.

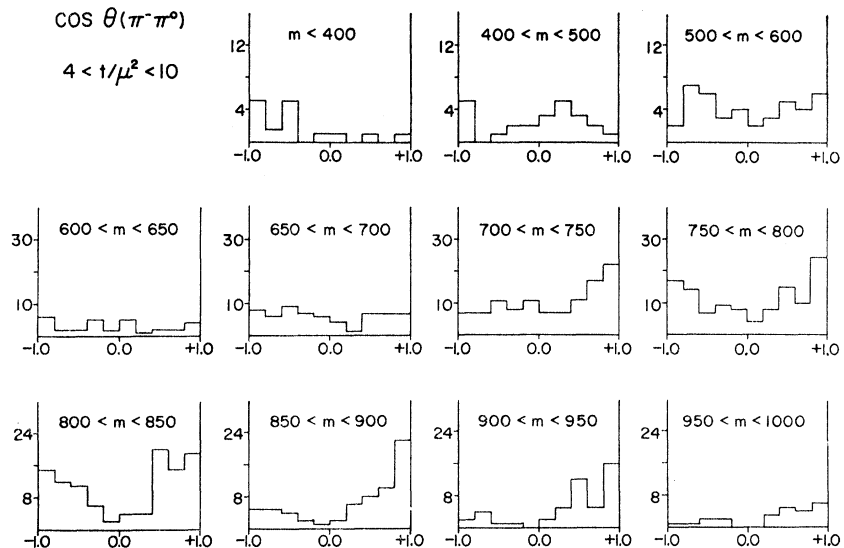


FIG. 27. $\cos\theta(\pi^-\pi^0)$ distributions, $4 < -t/\mu^2 < 10$.

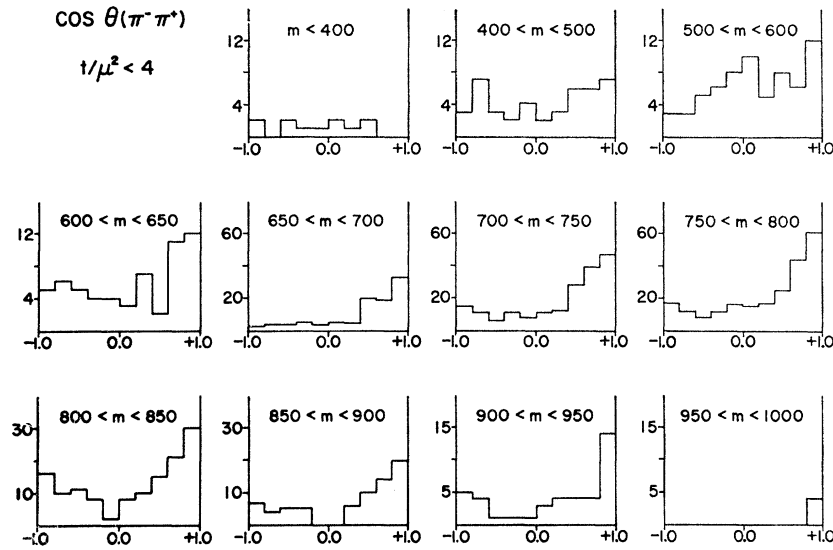


FIG. 28. $\cos\theta(\pi^-\pi^+)$ distributions, $-t/\mu^2 \leq 4$.

We have fit the total pion-pion mass distribution by the method of least squares to such a distribution function (assuming incoherence) with the results shown in Table III.

Several alternative assumptions were made about the shape of the resonance peak. The results are not in good agreement, although qualitatively they are similar. Note especially that in each space case ρ^0 production is twice that of ρ^- , which is just the expected result for a $T=1$ resonance formed in a peripheral collision.

Since none of the assumed resonance shapes fits the data well (especially the corrected p -wave Breit-Wigner shape which might be expected to be the best fit of the decay of the ρ), we will only note that most of the parameters agree qualitatively with other experi-

ments and also with what would be expected from simply observing the raw data (Figs. 16–23). The poor quantitative agreement most probably is due to incorrect assumptions, such as a phase-space background which is incoherent with a pure resonance.

The ρ production cross sections obtained (using Table I) reflect the theoretical uncertainties in the fits. Approximately, we obtain

$$\begin{aligned}\sigma(\pi^-p \rightarrow \rho^-p) &\approx 1.7 \text{ mb}, \\ \sigma(\pi^-p \rightarrow \rho^0n) &\approx 3.5 \text{ mb}.\end{aligned}$$

However, since these values are sensitive to the assumptions used in obtaining them, they should be regarded as uncertain.

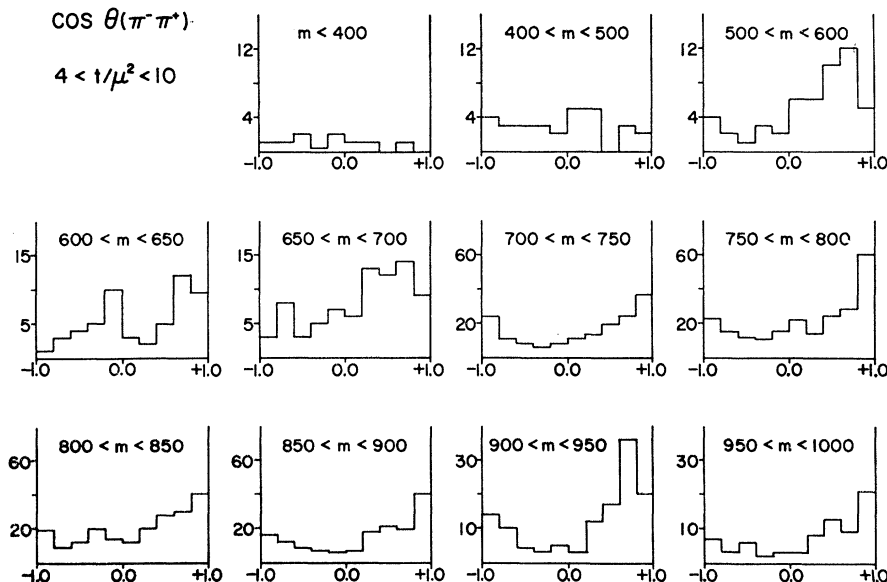


FIG. 29. $\cos\theta(\pi^-\pi^+)$ distributions, $4 < -t/\mu^2 \leq 10$.

TABLE III. ρ parameters from a fit to phase space plus an incoherent resonance form. The various assumptions for production amplitudes were: (a) Breit-Wigner: $|A|^2 \sim (\Gamma/2)/[(\omega_R - \omega)^2 + (\Gamma/2)^2]$. (b) Relativistic Breit-Wigner is the same as (a) except that $(\Gamma/2) \rightarrow \Gamma(q/q_R)^3/[1 + (q/q_R)^2]$, where q is the pion momentum in the ρ rest frame. (c) Gaussian: $|A|^2 \sim \exp[-(\omega_R - \omega)^2/2(\Gamma/2)^2]$. The correction applied was to take into account the effect on the resonance amplitude of the phase-space factor ωq . The number of degrees of freedom is 86 for $\pi^-\pi^0$ events and 87 for $\pi^-\pi^+$ events.

Resonance form	Charge state	f_ρ fraction in ρ	m_ρ (MeV)	Γ_ρ (MeV)	χ^2	$\sigma(\pi^-p \rightarrow \rho N)$ (mb)
Breit-Wigner	$\pi^-\pi^0$	0.60 ± 0.03	771 ± 3	171 ± 13	76	1.99 ± 0.11
	$\pi^-\pi^+$	0.72 ± 0.03	789 ± 3	198 ± 11	146	4.13 ± 0.18
B-W (corrected)	$\pi^-\pi^0$	0.57 ± 0.03	749 ± 3	149 ± 13	94	1.90 ± 0.10
	$\pi^-\pi^+$	0.67 ± 0.03	760 ± 3	173 ± 13	106	3.80 ± 0.15
P-wave	$\pi^-\pi^0$	0.50 ± 0.02	749 ± 3	109 ± 6	180	1.66 ± 0.08
Breit-Wigner	$\pi^-\pi^+$	0.59 ± 0.02	762 ± 2	127 ± 2	246	3.34 ± 0.12
	$\pi^-\pi^0$	0.42 ± 0.02	747 ± 3	69 ± 5	334	1.40 ± 0.07
P B-W (corrected)	$\pi^-\pi^+$	0.51 ± 0.02	760 ± 2	80 ± 4	246	2.89 ± 0.10
	$\pi^-\pi^0$	0.43 ± 0.02	770 ± 3	167 ± 9	94	1.43 ± 0.07
Gaussian	$\pi^-\pi^+$	0.49 ± 0.02	788 ± 3	180 ± 7	200	2.79 ± 0.10
	$\pi^-\pi^0$	0.43 ± 0.02	750 ± 3	169 ± 9	94	1.43 ± 0.07
G (Corrected)	$\pi^-\pi^+$	0.49 ± 0.02	765 ± 3	183 ± 7	199	2.79 ± 0.10

B. Pion-Pion Cross Section

1. Total Cross Section

The one-pion-exchange model was discussed in Sec. III. The results of this experiment clearly substantiate the view that at least in the region of the ρ meson the OPE model dominates the single-pion production process. In Sec. IV it was seen that low-momentum-transfer events are very important and that there is approximate isotropy in the Treiman-Yang angular distribution.

On the basis of one or the other of the OPE models, it is possible to infer approximately the free-particle pion-pion scattering cross section. The results are presented in Table IV on the basis of three different versions of the Chew-Low formula [Eqs. (8) and (12)],

the original Chew-Low formula, and the Selleri modifications for $l=0$ and $l=1$.

Presumably the Selleri formula for $l=1$ should be most accurate in the region of the ρ and in fact it does result in a pion-pion cross section near that expected for a pure $J=1$ resonance [$\sigma_{\max}(J=1) = 12\pi\lambda^2 = 121.6$ mb at 750 MeV]. Note that both the $\pi^-\pi^0$ and the $\pi^-\pi^+$ are close to the same value. This is a reflection of the $T=1$ nature of the ρ .

Below the region dominated by the ρ the interpretation of these data is more uncertain. Although we might assume that s -wave π - π scattering dominates and choose the Selleri formula for $l=0$, the effect of competing processes should be much more significant. That is, the OPE diagram may not dominate the contributions from other diagrams, e.g., those containing a pion-nucleon

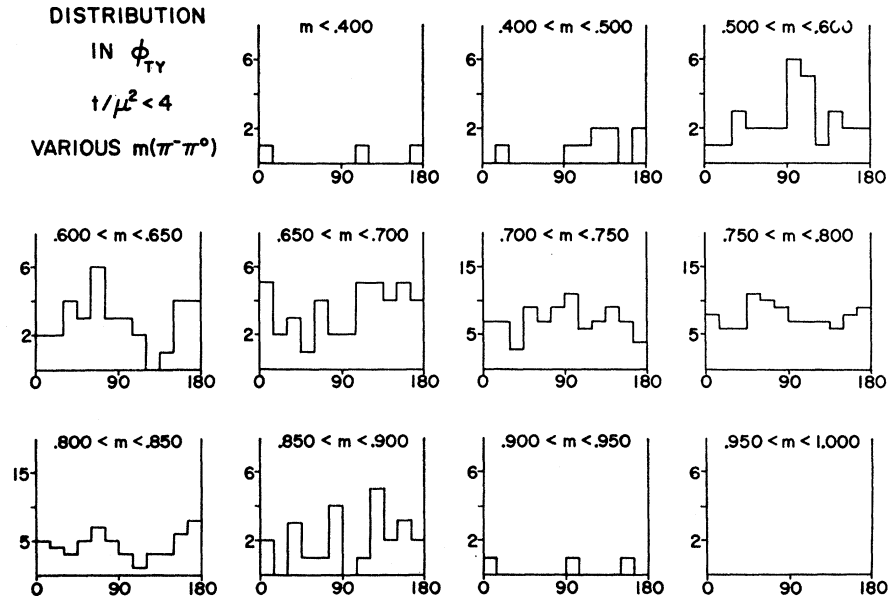


FIG. 30. Trieman-Yang angular distributions for $-t/\mu^2 \leq 4$. The ϕ_{TY} used in these graphs is 180° out of phase with the usual definition (see text).

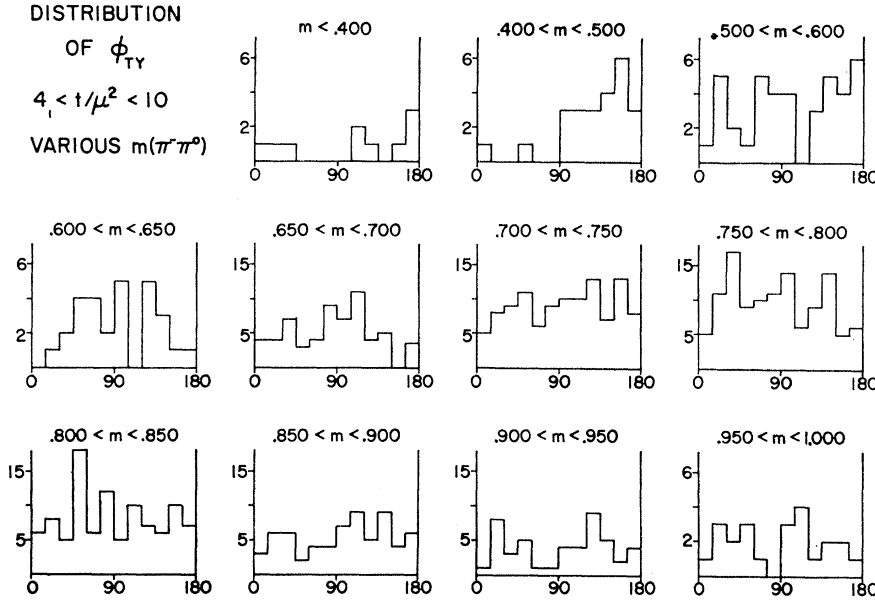


FIG. 31. $\phi_{TY}(\pi^-\pi^0)$,
 $4 < -t/\mu^2 \leq 10$.

scattering vertex [Figs. 11(b) and 11(c)]. This will be discussed further in Sec. VC.

The extrapolation procedure was carried out using only the data for $-t < 10\mu^2$ as suggested by Selleri. In the case of the $\pi^-p\pi^0$ final state there appears to be a deficiency of events with very low momentum transfer compared to $\pi^-\pi^+n$ events. Since this may be due to a scanning bias against very short protons similar to that for elastic events (even though the topologies are usually not alike), the condition was arbitrarily imposed

for the $\pi^-p\pi^0$ state that $4\mu^2 < -t < 10\mu^2$, whereas no lower limit on $-t$ was used for the $\pi^-\pi^+n$ state. In both cases the data were divided into bins $2\mu^2$ wide. The errors presented in Table IV are those resulting from the purely statistical errors assigned to the number of events in each bin.

TABLE IV. Pion-pion cross sections calculated from (1) original Chew-Low formula, (2) Selleri formula ($l=0$), and (3) Selleri formula ($l=1$).

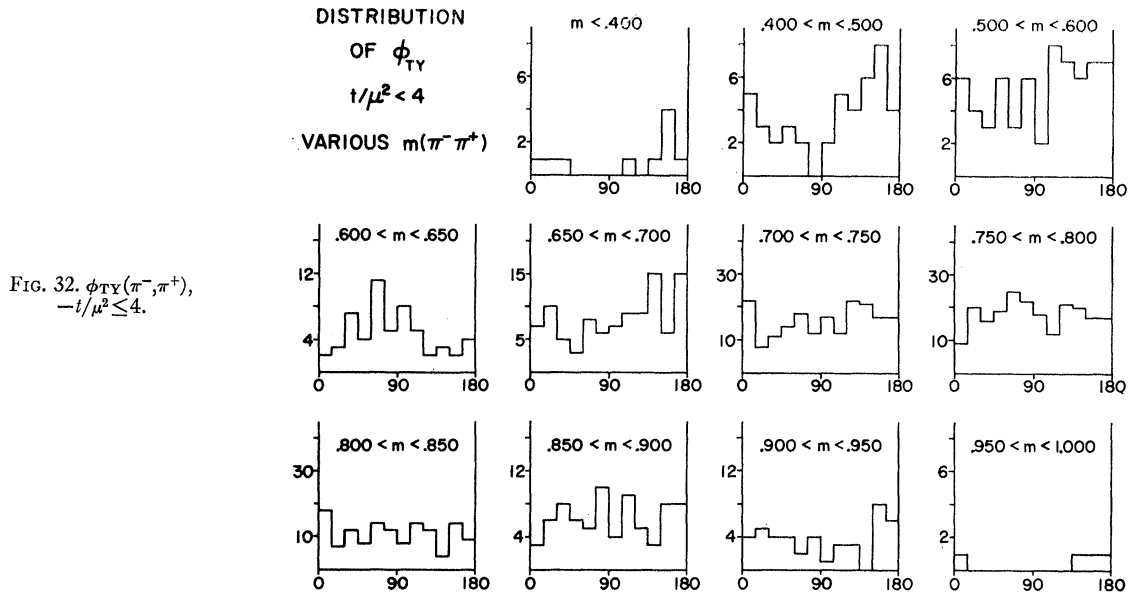
Type	Mass (BeV)	$\pi^-\pi^0$ cross sections		
		ρ_{CL} (mb)	$\sigma_S(l=0)$ (mb)	$\sigma_S(l=1)$ (mb)
$\pi^-\pi^0$	0.344	35 ± 10	107 ± 31	9 ± 3
	0.453	25 ± 5	75 ± 16	21 ± 4
	0.552	28 ± 4	92 ± 13	34 ± 5
	0.625	30 ± 5	94 ± 15	45 ± 7
	0.675	41 ± 5	138 ± 16	69 ± 8
	0.725	61 ± 5	193 ± 17	112 ± 10
	0.775	52 ± 4	171 ± 14	104 ± 9
	0.825	35 ± 3	112 ± 10	73 ± 7
	0.875	19 ± 2	64 ± 7	44 ± 5
	0.925	11 ± 2	37 ± 5	26 ± 4
0.975	6 ± 1	19 ± 4	14 ± 3	
$\pi^-\pi^+$	0.344	12 ± 3	29 ± 7	3 ± 1
	0.453	20 ± 2	47 ± 6	16 ± 2
	0.552	19 ± 2	42 ± 4	23 ± 2
	0.625	24 ± 2	55 ± 5	34 ± 3
	0.675	31 ± 2	77 ± 6	49 ± 4
	0.725	46 ± 3	123 ± 7	80 ± 4
	0.775	55 ± 3	147 ± 7	102 ± 5
	0.825	39 ± 2	105 ± 6	76 ± 4
	0.875	24 ± 2	70 ± 5	50 ± 3
	0.925	16 ± 1	53 ± 4	37 ± 3
0.975	8 ± 1	28 ± 3	20 ± 2	

2. Angular Distribution

The angular distribution data for events which are mainly ρ are approximately isotropic in the Treiman-Yang angle and have a $\cos^2\theta$ dependence for the pion scattering angle, all of which supports the OPE model and a $J=1$ pion-pion interaction. However, pure OPE predicts there should be no correlation between ϕ_{TY} and $\cos\theta_{\pi\pi}$ such as is seen in the scatter diagram of Fig. 34 and is discussed in Sec. IV.

These correlations are possible in the context of OPE only if absorption effects are included. In this case the angular distributions are given by Eq. (14) with ρ_{11} , ρ_{10} , $\rho_{1,-1}$ nonzero. Those spin-space density matrix elements which most accurately represent our data have been determined by a least-squares fit for various ranges of ρ production angle and are shown in Table V. (Please note that the sign of ρ_{10} is opposite to that which it would have if ϕ_{TY} had been defined in the usual way. Apparent discrepancies between this and other experiments will result if this fact is not taken into account.) The data are averaged over a range of $M(\pi^-\pi^0)$ from 680 to 850 MeV. No corrections for background have been made.

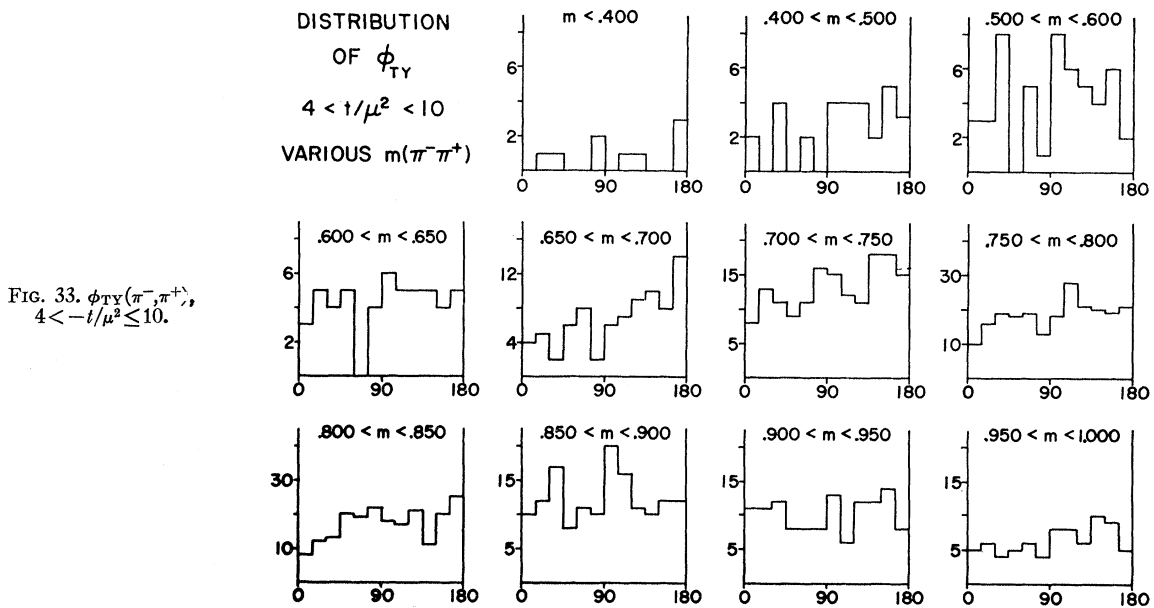
The pure OPE model, of course, predicts that only ρ_{00} is different from zero. One of the triumphs of the OPE model with absorption (OPEA) is that fairly accurate predictions have been made for the matrix elements



for various experimental situations.²¹ The results given in Table V for the $\pi^-\pi^0$ data agree within errors with the values predicted by the model of Jackson and his collaborators.²²

A comparison of the theory with our $\pi^-\pi^0$ data is shown in Fig. 47. The solid curves marked $\lambda=0$ are the results of Jackson's computations for this OPEA model. His calculations also allow for possible ω^0

exchange as a mechanism for ρ^- production. This is done in terms of λ , the ratio of the coupling constants $g_{\pi\omega\rho}$ and $g_{\pi\rho\rho}$. The matrix element which is most sensitive to this parameter, ρ_{00} , seems to be best fit with the predictions for $\lambda=0$. Thus, in this experiment ρ^- production can be well understood in terms of a pion-pion interaction including the effects of absorption in the initial and final states, but with no ω^0 exchange.



²¹ A review of some of the data is given in J. D. Jackson, Rev. Mod. Phys. 37, 484 (1965).

²² Many thanks are due Dr. Jackson and his collaborators (especially Jerry Hite) for making these data available. The parameters used in the calculations were $C_1=0.95$, $\gamma_1=0.083$, $C_2=1.0$, and $\gamma_2=0.083$. Reference 21 explains the significance of these quantities.

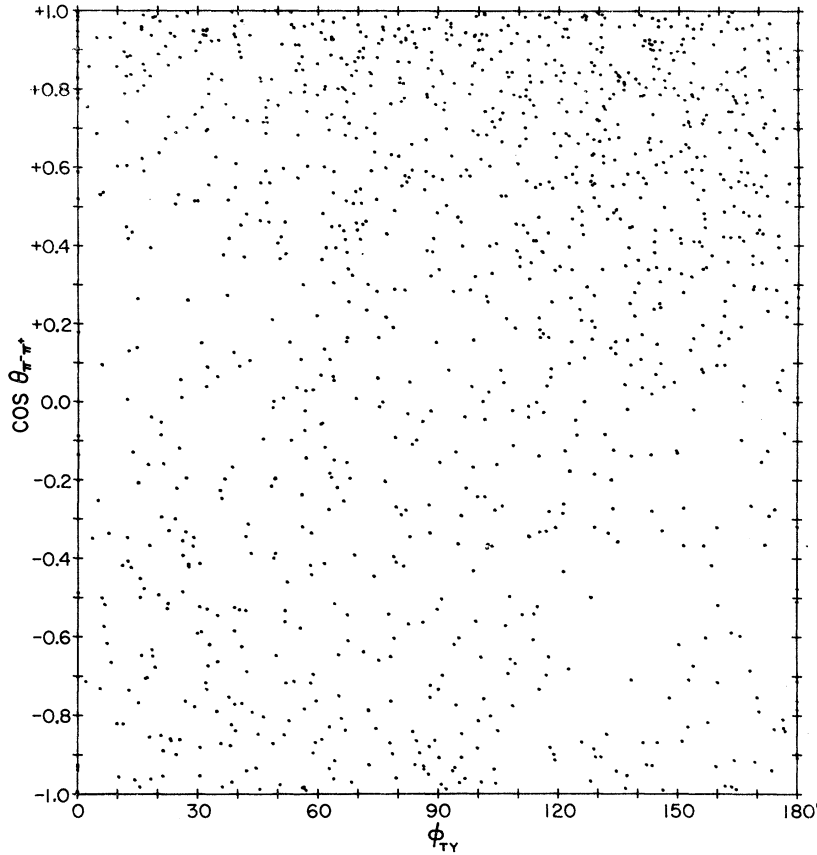


FIG. 34. Scatter diagram of $\cos\theta(\pi^-, \pi^+)$ and ϕ_{TY} , $700 < M(\pi^-, \pi^+) < 850$ MeV, $-t/\mu^2 < 10$.

The $\pi^-\pi^+$ data are not in agreement with the calculations of Jackson, and in fact only very bad fits to Eq. (14) were possible. This is due to the forward scattering effect which this model does not predict either with or without absorption.

3. Existence of a $T=0$ Resonance

So far the forward peaking in the $\cos\theta(\pi^-\pi^+)$ distribution has not been explained. Equation (16) shows that the OPEA model predicts an isotropic term in addition to the $\cos^2\theta$ dependence, but asymmetric terms do not appear. In order to explain such behavior it has been suggested that there exists a $T=0$, s -wave, π - π resonance (denoted by ϵ^0 , mass ~ 730 MeV, width ~ 100 MeV) which interferes with the ρ decay angular

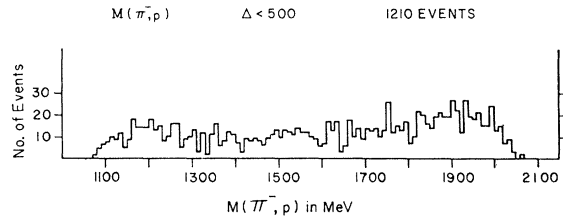
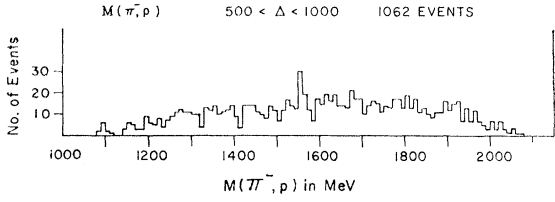
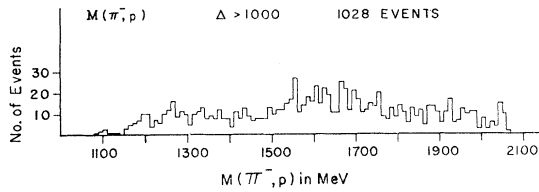
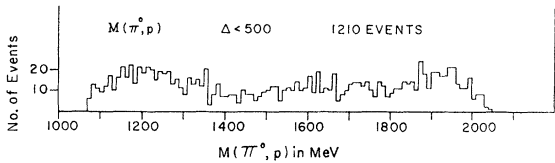
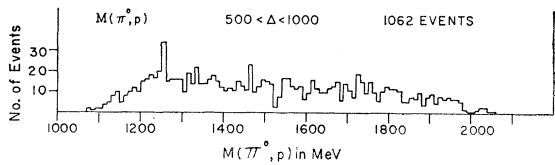
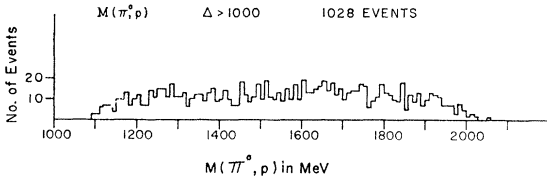


FIG. 35. Pion-nucleon mass distributions $M(\pi^-\rho)$, $\Delta \leq 500$ MeV/c.

distribution, but is obscured in a mass plot since the spin factors and isotropic-spin Clebsch-Gordan coefficients combine to reduce its maximum contribution to about 15% that of the ρ^0 . Evidence favoring this hypothesis has been presented in terms of a density

TABLE V. Spin-space density matrix elements for ρ decay assuming no background or interference. The sign of ρ_{10} is opposite to the usual notation. Averaging is for $680 < M(\pi\pi) < 850$ MeV.

Charge	$\pi^-\pi^0$					$\pi^-\pi^+$						
$\cos\theta$	1.0	-0.98	0.98	-0.95	0.95	-0.90	1.0	-0.98	0.98	-0.95	0.95	-0.90
ρ_{00}		0.812 ± 0.059		0.784 ± 0.050		0.636 ± 0.046		0.632 ± 0.035		0.620 ± 0.032		0.526 ± 0.038
ρ_{11}		0.094 ± 0.029		0.108 ± 0.025		0.182 ± 0.023		0.184 ± 0.018		0.190 ± 0.016		0.237 ± 0.019
$\text{Re } \rho_{10}$		0.074 ± 0.037		0.053 ± 0.032		0.078 ± 0.026		0.189 ± 0.019		0.143 ± 0.017		0.144 ± 0.019
$\rho_{1,-1}$		0.040 ± 0.039		-0.005 ± 0.032		0.111 ± 0.031		-0.072 ± 0.026		0.051 ± 0.024		0.073 ± 0.025
χ^2		27.5		24.5		47.5		146		148		112

FIG. 36. $M(\pi^-, p)$, $500 < \Delta \leq 1000$ MeV/c.FIG. 37. $M(\pi^-, p)$, $\Delta > 1000$ MeV/c.FIG. 38. $M(\pi^0, p)$, $\Delta \leq 500$ MeV/c.FIG. 39. $M(\pi^0, p)$, $500 < \Delta \leq 1000$ MeV/c.FIG. 40. $M(\pi^0, p)$, $\Delta > 1000$ MeV/c.

matrix analysis by Durand and Chiu²³ and Derado *et al.*²⁴ and raw experimental results containing certain anomalies in the region of the ρ by Hagopian *et al.*²⁵

Equation (18) predicts the form of the decay angular distribution of the combined ρ^0 , ϵ^0 system. Table VI shows the matrix elements obtained by a least-squares fit to our data. As a check the $\pi^-\pi^0$ data were fit to the same distribution with the result that the terms corresponding to the presence of an ϵ^0 are consistent with

²³ L. Durand, III, and Y. T. Chiu, Phys. Rev. Letters **14**, 329 (1965).

²⁴ I. Derado, V. P. Kenney, J. A. Poirier, and W. D. Shephard, Phys. Rev. Letters **14**, 872 (1965).

²⁵ W. Hagopian, W. Selove, J. Alliti, J. P. Baton, and M. Neveu-Rene, Phys. Rev. Letters **14**, 1077 (1965).

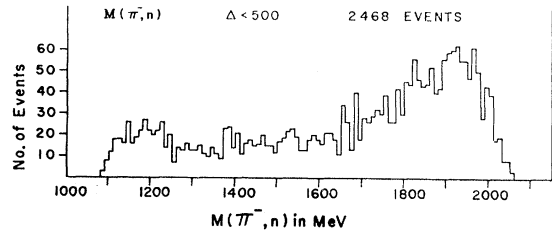
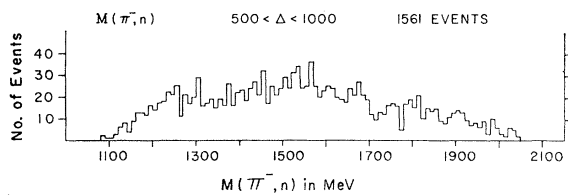
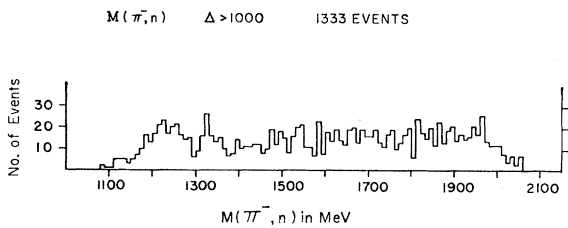
zero and the χ^2 value is improved only slightly. This is to be expected, of course, since the $\pi^-\pi^0$ system is charged and has no $T=0$ component.

On the other hand, a sizable improvement was observed in the fits for $\pi^-\pi^+$ (although they are still not good). These fits are similar to those obtained by Derado *et al.*²⁴ with 4-BeV/c π^- incident on p . (The signs of $\langle a_1 a_0 \rangle$ and $\langle a_1 b_0 \rangle$ are opposite owing to the different definition of $\phi_{\pi\gamma}$.) In particular the forward peaking in the $\cos\theta(\pi^-\pi^+)$ distribution produces a fairly sizable $\langle a_0 b_0 \rangle$ term.

Figure 48 shows graphically the values obtained in the fit of the data to Eq. (18). These are the same as are shown in Table VI. A theoretical calculation of these quantities by Durand and his collaborators²⁶ is now under way.

The experimental ambiguity in determining the matrix elements (mentioned in Sec. III) was resolved by arbitrarily setting $\langle b_0 b_0 \rangle$ equal to zero. (A small correction for a nonzero value is easily made.) This then fixed the values for $\langle a_0 a_0 \rangle$ and $\langle a_1 a_1 \rangle$.

Although the ϵ^0 hypothesis explains the qualitative aspects of our data, the poor fits for ρ^0 decay suggest that there may be other effects which have not been

FIG. 41. $M(\pi^-, n)$, $\Delta \leq 500$ MeV/c.FIG. 42. $M(\pi^-, n)$, $500 < \Delta \leq 1000$ MeV/c.FIG. 43. $M(\pi^-, n)$, $\Delta \geq 1000$ MeV/c.

²⁶ Many thanks are due Dr. Durand and his collaborators for making these calculations. Unfortunately they were not completed as this was written.

TABLE VI. Matrix elements for ρ decay allowing for interference with a $T=0$, s -wave pion-pion resonance. The signs of $\langle a_1 a_0 \rangle$ and $\langle a_1 b_0 \rangle$ are opposite to the usual notation. The value of $\langle b_0 b_0 \rangle$ is taken as zero in order to compute $\langle a_0 a_0 \rangle$ and $\langle a_1 a_1 \rangle$ uniquely. For a nonzero value of $\langle b_0 b_0 \rangle$ subtract $\langle b_0 b_0 \rangle/3$ from each of the given values of $\langle a_0 a_0 \rangle$ and $\langle a_1 a_2 \rangle$. The number of degrees of freedom is 24.

Charge: $\cos\gamma_p$:	$\pi^-\pi^0$ 1.0-0.98	$\pi^-\pi^0$ 0.98-0.95	$\pi^-\pi^0$ 0.95-0.90	$\pi^-\pi^+$ 1.0-0.98	$\pi^-\pi^+$ 0.98-0.95	$\pi^-\pi^+$ 0.95-0.90
$\langle a_0 a_0 \rangle$	0.807 ± 0.059	0.784 ± 0.050	0.609 ± 0.047	0.701 ± 0.036	0.660 ± 0.033	0.578 ± 0.038
$\langle a_1 a_1 \rangle$	0.096 ± 0.029	0.108 ± 0.025	0.166 ± 0.023	0.149 ± 0.098	0.170 ± 0.016	0.211 ± 0.019
$\langle a_1 a_0 \rangle$	0.074 ± 0.037	0.065 ± 0.033	0.076 ± 0.026	0.120 ± 0.021	0.126 ± 0.019	0.152 ± 0.019
$\langle a_1 a_1 \rangle$	0.042 ± 0.039	-0.006 ± 0.032	0.093 ± 0.031	-0.044 ± 0.026	0.027 ± 0.024	0.062 ± 0.026
$\langle a_1 b_0 \rangle$	0.009 ± 0.021	0.003 ± 0.019	0.006 ± 0.016	0.003 ± 0.015	0.042 ± 0.013	0.062 ± 0.013
$\langle a_0 b_0 \rangle$	0.031 ± 0.048	0.013 ± 0.042	0.141 ± 0.036	0.259 ± 0.026	0.251 ± 0.025	0.207 ± 0.025
$\langle b_0 b_0 \rangle$	0.0	0.0	0.0	0.0	0.0	0.0
2	27.0	24.4	31.7	41.7	43.5	38.8

taken into account such as additional final-state interactions or non-OPE processes.

Hagopian *et al.*²⁵ present data from π^-p experiments at 2.75 and 3.0 BeV/c which support the ϵ^0 hypothesis in that several anomalies occur at just the proposed ϵ^0 mass. For example, they present a $\pi^-\pi^+$ mass histogram which peaks near 770 MeV with all events included, but peaks near 720 when only events with $|\cos\theta(\pi^-\pi^+)| < 0.3$ are included. For larger momentum transfer and for other charge states this effect does not occur. In this way they attempt to select events with an s -wave pion-pion interaction.

Our data are not in agreement with them on this point. Figure 49 shows that the distribution in $M(\pi^-\pi^+)$ for $|\cos\theta| < 0.3$ has no large peak at 720 MeV and in fact is very similar in shape to the distribution for all $\cos\theta$. This is exactly what the OPEA model predicts

since one of the main effects of the model is to produce an isotropic component in the $\cos\theta$ distribution. Thus a peak in $M(\pi^-\pi^+)$ will appear near the ρ mass regardless of restrictions imposed on the scattering angle.

Other arguments are put forward by Hagopian *et al.* in terms of sudden variations in scatter diagram distributions for $M(\pi^-\pi^+)$ near 720 MeV. However, it seems unlikely that any firm conclusions can be made with such qualitative and statistically marginal evidence. Other than direct observation of an ϵ^0 , the most fruitful approach would seem to be detailed analysis of the correlations and asymmetries in the decay of the ρ^0 .

Several experiments which could detect the $2\pi^0$ decay mode of the ϵ^0 have been performed. Strong evidence favoring the existence of the ϵ^0 has been ob-

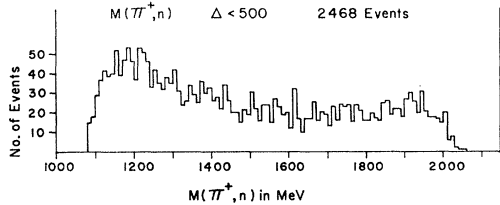


FIG. 44. $M(\pi^+, n)$, $\Delta \leq 500$ MeV/c.

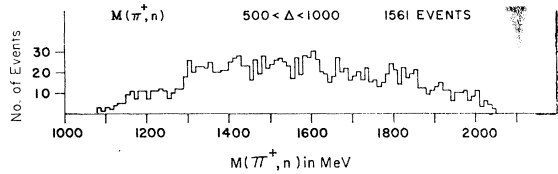


FIG. 45. $M(\pi^+, n)$, $500 < \Delta \leq 1000$ MeV/c.

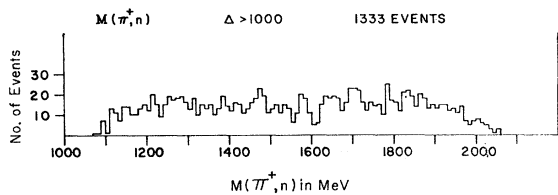
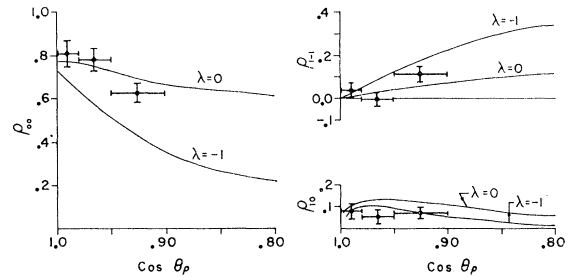
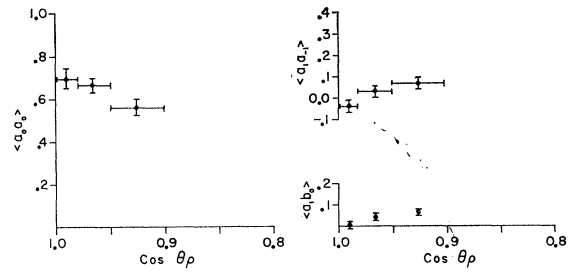


FIG. 46. $M(\pi^+, n)$, $\Delta > 1000$ MeV/c.



SPIN SPACE DENSITY MATRIX ELEMENTS
 $.680 < M(\pi^-\pi^0) < .850$

FIG. 47. Spin-space density matrix elements for $\pi^-\pi^0$ data averaged over the mass range 680-850 MeV. The solid curves are the calculations of Jackson *et al.* (see Ref. 22).



DECAY COEFFICIENTS FOR $\pi^-\pi^+$
 $.680 < M(\pi^-\pi^+) < .850$

FIG. 48. Coefficients in decay distribution for the combined $\rho^0 + \epsilon^0$ system.

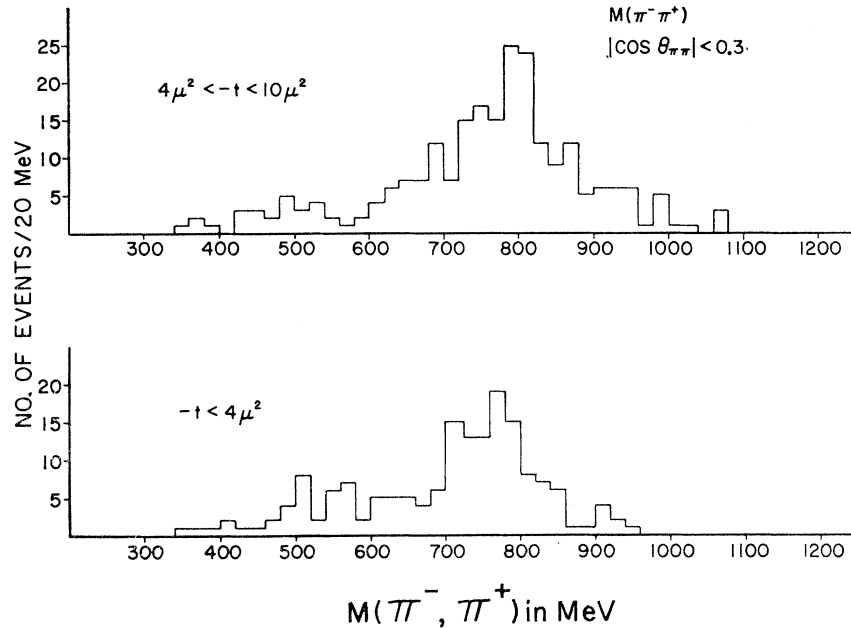


FIG. 49. Pion-pion mass distribution $M(\pi^-, \pi^+)$ for $\cos\theta(\pi^-\pi^+) < 0.3$ (a) $-t/\mu^2 \leq 4$, (b) $4 \leq -t/\mu^2 \leq 10$.

tained using spark chambers and a neutron time-of-flight technique. Feldman *et al.*²⁷ observed a sharp peak in the time-of-flight distribution corresponding to a recoiling mass of 700 MeV. That two neutral pions are involved is suggested by the fact that the peak is observed for events with four observed γ 's.

On the other hand, the e^0 should also be observable in the reaction $\pi^+d \rightarrow pp e^0$ as a peak in a missing mass plot. The experiment of Gelfand *et al.*²⁸ fails to show any evidence of a peak near 700 MeV. The missing mass distributions of the present experiment likewise show no significant enhancements near the presumed e^0 mass. A small bump does show up for events of the type $\pi^-p \rightarrow \pi^-p X^0$ (where X^0 is more than one neutral pion), but it is too insignificant statistically to be taken seriously.²⁹

At present direct experimental evidence for the e^0 is inconclusive. It may be necessary to seek other explanations for the asymmetry of the ρ^0 . It is worth noting that if the $T=0$, s -wave amplitude should have a large imaginary part then the asymmetry through the resonance would naturally follow. Whether this results from a phase shift of $\pm 90^\circ$ or strong absorption of the s -wave system is not known at present.

C. Pion-Nucleon Interactions

1. Effect on ρ^0 Decay

It has been suggested that one possible cause of ρ decay asymmetry would be a final-state interaction in

the π^-n system. As has been noted above with reference to the Dalitz plot for $\pi^-\pi^+n$ (Fig. 13), there is a kinematic correlation between an enhancement in the $\cos\theta(\pi^-\pi^+)$ distribution and one in the $M(\pi^-, n)$ distribution. Bussian and Oppenheimer³⁰ point out that at this energy the $T=\frac{3}{2}$ πN resonance at 1920 MeV is nearly on the mass shell. If the $N^*(1920)$ is copiously produced and the π^-n vertex behaved as if it were real particle two-body elastic diffraction scattering, then a strong forward peak would appear in the $\cos\theta(\pi^-, \pi^+)$ distribution for low momentum transfers.

If this were the mechanism which produces the ρ^0 decay asymmetry, then for different beam momenta the enhancement in $\cos\theta(\pi^-, \pi^+)$ associated with the $N^*(1920)$ would no longer occur in the forward direction, or if the diffraction scattering process continued, but was associated with a nonresonant π^-n interaction, then at least its magnitude would be reduced. Since the asymmetry occurs at all beam energies, we can say with confidence that the forward peaking in $\cos\theta$ is a property of the $\pi^-\pi^+$ system and is almost independent of any π^-n final-state interaction.

2. Existence of $\pi-N$ Final-State Interaction

However, there do seem to be significant enhancements in the (π^-, n) distributions.³⁰⁻³² To examine the π^-n system without complications due to the effects of the ρ^0 , Fig. 50 shows the distributions of $M(\pi^-, n)$

²⁷ M. Feldman, W. Frati, J. Halpern, A. Kanofsky, M. Nussbaum, S. Richert, P. Yamin, A. Choudry, S. Devons, and J. Grunhaus, Phys. Rev. Letters **14**, 869 (1965).

²⁸ N. Gelfand, G. Lutjens, M. Nussbaum, J. Steinberger, A. O. Cohn, W. M. Buss, and G. T. Condo, Phys. Rev. Letters **12**, 568 (1964).

²⁹ J. Bishop, University of Wisconsin (private communication).

³⁰ A. E. Bussian and F. Oppenheimer, Phys. Rev. Letters **12**, 649 (1964).

³¹ E. West, W. D. Walker, J. Boyd, A. R. Erwin, and M. A. Thompson, Bull. Am. Phys. Soc. **9**, 639 (1964).

³² Lazlo Gutay, S. K. Tuli, J. R. Albright, and J. E. Lanutti, Bull. Am. Phys. Soc. **9**, 639 (1964). L. J. Gutay, J. E. Lanutti, P. L. Csonka, M. J. Moravcsik, and M. D. Scadron, Phys. Letters **16**, 343 (1965).

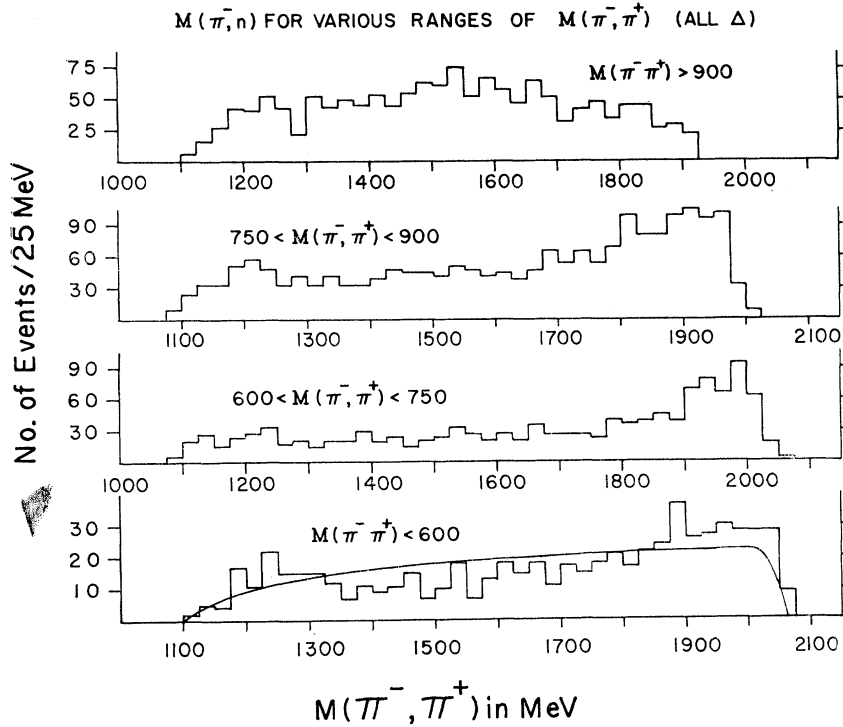


FIG. 50. $M(\pi^-, n)$ for various ranges of $M(\pi^-, \pi^+)$ for all momentum transfers. The phase-space curve drawn for $M(\pi^-, \pi^+) < 600$ MeV is normalized to the total number of events.

for several ranges of $M(\pi^-, \pi^+)$. In particular, for pion-pion masses below the ρ , enhancements appear at both the low- and high-end of the spectrum. These clearly significant peaks are probably the $N^*(1238)$ and the $N^*(1920)$.

Such isobars may result from diagrams such as Fig. 11(b) in which a nucleon rather than a pion is the exchanged particle. This possibility was tested by Bussian and Oppenheimer³⁰ by means of a Treiman-Yang plot in which they plotted the angle α defined by

$$\cos\alpha = \frac{\mathbf{q}_1 \times \mathbf{K} \cdot \mathbf{q}_2 \times \mathbf{P}_1}{|q_1 \times K| |q_2 \times P_1|}$$

as evaluated in the isobar rest frame. [See Fig. 11(b) for variable definition.] While any interaction which proceeds purely by means of the nucleon exchange diagram will yield a uniform distribution in α , interference with some other process (such as OPE) may produce nonuniformity. This has been detected by Bussian and Oppenheimer,³⁰ Gutay *et al.*,³² and also in this experiment.³¹

However, the results of this experiment are in conflict with those of Bussian and Oppenheimer in that their distribution in α peaks at 180° , while in this experiment there is a peak at 0° . Figure 51 shows the distribution in α for various ranges of $M(\pi^-, n)$ with " ρ events" cross hatched. [In this case " ρ events" means $700 < M(\pi^-, \pi^+) < 800$ MeV and $\Delta < 500$ MeV/c. This is the definition used in Ref. 30.]

Apparently the nucleon exchange diagram becomes more important for higher π^-n masses. This may be due to the fact that for the energy of this experiment the

higher massed isobar is closest to being on the mass shell (see Ref. 30). This could explain the comparative insignificance of the $N^*(1238)$.

Finally, it seems clear that while final-state pion-nucleon interactions do not dominate, they do exist and should be taken into account in the analysis of any process which itself is not completely dominant. An understanding of the ρ meson may be obtained while ignoring all other features of the data. However, any analysis of pion-pion s -wave scattering must allow for effects such as baryon exchange.

3. Pion-Pion s -Wave Scattering

Since an understanding of s -wave pion-pion interactions requires that we take into account pion-nucleon interactions, we have computed the expected $\pi^+\pi^-$ mass distribution using the model described in Sec. III E and Appendix A. After normalizing to account for absorption effects [which we assume are independent of $M(\pi^-, \pi^+)$] a comparison was made with the data for various assumed values of the $T=0$, s -wave pion-pion cross section. Here we ignored the $T=2$ cross section which several experiments³³ indicate is very small in the region of the ρ and below.

³³ The study of $\pi^-p \rightarrow \pi^-\pi^+\pi^0$ from this experiment [see Ref. 7 or P. H. Satterblom, W. D. Walker, and A. R. Erwin, Phys. Rev. 134, B207 (1964)] shows no evidence of any strong $T=2$ pion-pion interaction. The same result is obtained in the Aachen-Berlin-Birmingham-Bonn-Hamburg-London (I.C.)-München collaboration, Phys. Rev. 138, B897 (1965) in which they investigated the $\pi^+\pi^+$ interaction from the process $\pi^+p \rightarrow \pi^+\pi^0n$. Also see Saclay-Orsay-Bari-Bologna collaboration, Nuovo Cimento 35, 1 (1965).

TREIMAN-YANG ANGLE FOR BARYON EXCHANGE

■ - "p EVENTS"

FIG. 51. Trieman-Yang angle for Baryon exchange (for definition of α see text).

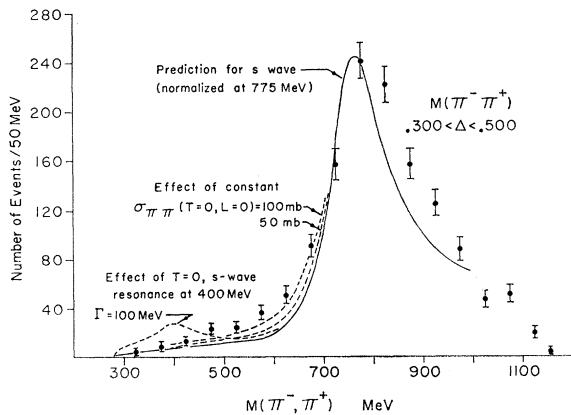
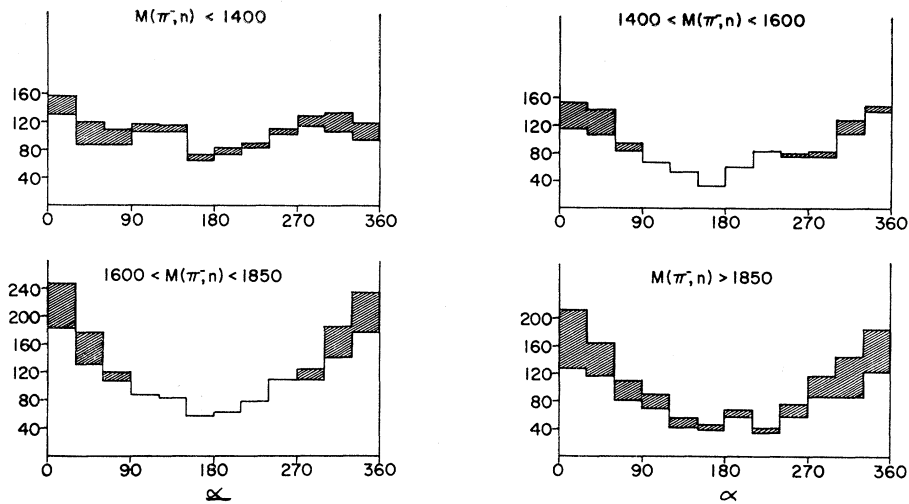


FIG. 52. Comparison of $M(\pi^-, \pi^+)$, $\Delta < 300$ MeV/c, with model including corrections due to pion-nucleon interactions.

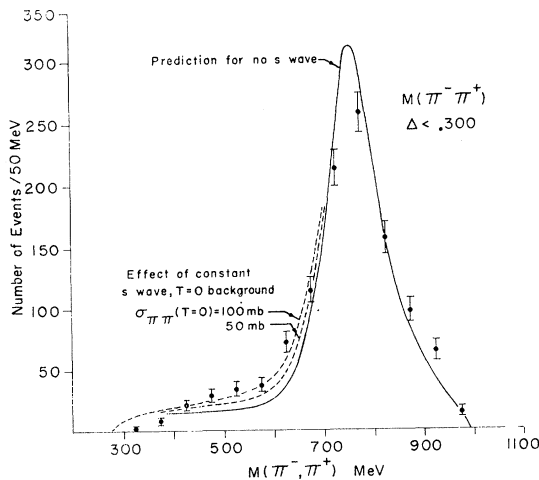


FIG. 53. Comparison of $M(\pi^-, \pi^+)$, $300 < \Delta < 500$ MeV/c, with the model.

Figures 52 and 53 show that with no s -wave interaction the non-OPE terms produce a fairly constant background which accounts for a large fraction of the events with low $M(\pi^-\pi^+)$. In fact in the region of very small momentum transfer and $M(\pi^-\pi^+) < 400$ MeV, there are significantly fewer events than predicted by this model. This scarcity of events is also clearly discernible in the $\pi^-\pi^+$ Chew-Low plot (Fig. 15). We have no explanation for this effect, although experimental biases or interference between production amplitudes could produce such effects.

Including s -wave terms (shown as broken lines on Figs. 52 and 53) indicates that between 450 and 650 MeV the $T=0$ s -wave total cross section is about 100 to 150 mb. Since the Clebsch-Gordan coefficient relating this to $\sigma(\pi^-\pi^+)$ is one-ninth we can say that the $\pi^-\pi^+$ cross section in this energy range is about 10 to 15 mb with statistical errors of the order of 50%. This result implies that we should disregard the values of $\sigma(\pi^-\pi^+)$ obtained by the extrapolation method (Sec. VB and Table IV) which do not take into account any non-OPE background.

Finally it should be noted that these results can be accepted only qualitatively since several approximations were made in the analysis. However, these values of the cross section are probably better than those obtained by the extrapolation procedure. It is to be hoped that a more rigorous computation may yield a reliable and accurate method of determining low-energy pion-pion cross sections.

ACKNOWLEDGMENTS

We wish to acknowledge the generous help of Dr. R. K. Adair and Dr. L. Leipuner in the operation of the bubble chamber. We wish also to acknowledge the Cosmotron crew and administrative staff, in particular

E. Dexter, for their aid in making this work possible. We thank various people at Wisconsin for scanning, measuring, and bookkeeping help, in particular, G. Thoreson, J. Myers, A. Rhombert, R. Liu, and R. Fuller. We also wish to acknowledge the programming help of Dr. R. Hartung, Dr. R. March, and Dr. M. Thompson and to thank Professor C. Goebel and Professor L. Durand for helpful discussions.

APPENDIX A: APPROXIMATE FIELD THEORY CALCULATION OF $\pi^-p \rightarrow \pi^- \pi^+ n$

The three lowest order Feynman diagrams which contribute to single-pion production are shown in Fig. 11. For events with small four-momentum transfer to the nucleon the single-pion-exchange diagram (a) is expected to dominate. Moreover, diagrams (b) and (c) tend to cancel each other out. In the approximation in which only diagram (a) contributes a calculation of the cross section leads directly to the well-known Chew-Low formula.

The experimental data, however, contain clear indications that other matrix elements do make significant contributions to the cross section. To investigate these deviations from pure single pion exchange, we compute here, approximately, the effect of diagrams (b) and (c) in which we take account of pion-nucleon diffraction scattering.

The invariant matrix element for diagram (a) is given by³⁴

$$T_a = \bar{u}(p) g\gamma_5 [1/(t-\mu^2)] F u(p'), \quad (\text{A1})$$

where $g\gamma_5$ is the $pn\pi^+$ coupling, $t = (p-p')^2$ is the four-momentum transfer to the nucleon squared, μ = pion mass, F = invariant pion-pion scattering amplitude (a scalar), and $u(p)$ = Dirac spinor for a nucleon of four-momentum p [normalized so that $\bar{u}(p)u(p) = 2m$]. Also F is connected to the usual nonrelativistic scattering amplitude f by

$$F = 8\pi\omega f, \quad (\text{A2})$$

where ω is the dipion invariant mass.

Contraction of the matrices in Eq. (A1) yields

$$T_a = [igF/(t-\mu^2)] \langle \bar{\chi}' | \boldsymbol{\sigma} \cdot \mathbf{V}_a | \chi \rangle, \quad (\text{A3})$$

where the matrix element is expressed in terms of two-component spinors, Pauli spin matrices, and

$$\mathbf{V}_a = \left(\frac{P_0+m}{P_0'+m} \right)^{1/2} \mathbf{P}' - \left(\frac{P_0'+m}{P_0+m} \right)^{1/2} \mathbf{P}. \quad (\text{A4})$$

The other two diagrams contain pion-nucleon scattering as subvertices which we approximate with the amplitude

$$T_{\pi N} = A_{\pi N} \begin{pmatrix} 1 & 0 \\ 0 & 0 \end{pmatrix}, \quad (\text{A5})$$

³⁴ The normalization used here is the same as those used in P. T. Mathews, 1963 Brandeis Lectures, Vol. I, 1964 (unpublished).

which suppresses the antinucleon intermediate states and in effect assumes that the nucleon is nonrelativistic. In addition, the optical theorem provides a knowledge of the behavior of $\text{Im}(A_{\pi N})$, since the cross sections have been well measured in this energy region. Thus we have

$$\text{Im}(A_{\pi N}) = 2P_c M \sigma(M) e^{d/d_0} / 2m, \quad (\text{A6})$$

where the $2m$ is included to maintain the proper normalization, and where M = invariant mass of π^- -neutron system, and $d = (K-q_1)^2$ is the square of the four-momentum transfer to the π^- . The term $\exp(d/d_0)$ is included to represent the behavior of diffraction scattering. The real part of $A_{\pi N}$ in this approximation can be computed from forward dispersion theory calculations. (The data used in these computations were obtained from Refs. 17 and 18.)

The amplitude corresponding to diagram (b) then is

$$T_b = \bar{u}(p) T_{\pi n} \frac{1}{\mathbf{p}' - \mathbf{q}_2 - m} g\gamma_5 u(p) \\ = \frac{igA_{\pi n}(M,d)}{r-m^2} \langle \bar{\chi}' | \boldsymbol{\sigma} \cdot \mathbf{V}_b | \chi \rangle, \quad (\text{A7})$$

where $r = (P' - q_2)$ is a scalar; and

$$\mathbf{V}_b = [(P_0+m)(P_0'+m)]^{1/2} \left[\mathbf{q}_2 + \frac{q_{20}}{P_0'+m} \mathbf{P}' \right]; \quad (\text{A8})$$

similarly, diagram (c) contributes

$$T_c = \frac{igA_{\pi n}(W,d)}{h-m^2} \langle \bar{\chi}' | \boldsymbol{\sigma} \cdot \mathbf{V}_c | \chi \rangle, \quad (\text{A9})$$

where $h = (P+q_2)^2 = M^2$, W = total center-of-momentum energy, and

$$\mathbf{V}_c = [(P_0+m)(P_0'+m)]^{1/2} \left[\mathbf{q}_2 - \frac{q_{20}}{P_0+m} \mathbf{P} \right]. \quad (\text{A10})$$

Now the total amplitude is given by

$$T = ig \langle \bar{\chi}' | \boldsymbol{\sigma} \cdot \mathbf{V} | \chi \rangle, \quad (\text{A11})$$

where

$$\mathbf{V} = \frac{F_2}{t-\mu^2} \mathbf{V}_a + \frac{A_{\pi n}(Md)}{r-m^2} \mathbf{V}_b + \frac{A_{\pi p}(Wd)}{h-m^2} \mathbf{V}_c. \quad (\text{A12})$$

Straightforward but tedious calculation eventually results in the interaction rate

$$R = \frac{g^2 |\mathbf{V}|^2}{32(2\pi)^4 \omega^2} \frac{1}{4} \left(\frac{\omega^2}{4} - \mu^2 \right)^{1/2} \frac{d\omega^2 dt d\Omega}{\bar{P}'}, \quad (\text{A13})$$

where R is to be evaluated in the barycentric system of the two pions. The solid angle Ω refers to the angle of

scatter of the π^- as measured in that system. The cross section then is just rate/flux. In our normalization the invariant flux is just $4m\bar{K}_{\text{LAB}}$.

Finally it should be pointed out that the value computed for $|\mathbf{V}|^2$ must be that in the laboratory (or any system where the nucleon is nonrelativistic) since the approximation of Eq. (A5) essentially is to assume that the nucleon is nonrelativistic. But since the true $|\mathbf{V}|^2$ is an invariant this value will be a good approximation in any Lorentz frame. The calculation of the rate for any range of pion-pion mass, momentum transfer, or dipion decay direction can now be computed numerically for any assumed pion-pion scattering amplitude (see Appendix B) by means of numerical integration on a digital computer.

APPENDIX B: PION-PION SCATTERING AMPLITUDES

In considering the scattering of two pions it is convenient to analyze the data in terms of isotopic spin states as well as particle states. To this end we note that the usual scattering amplitude is

$$f(\theta) = \lambda \sum_l (2l+1) A_l P_l(\cos\theta), \quad (\text{B1})$$

where $A_l = e^{i\delta_l} \sin\delta_l$. Since even (odd) isotopic spin states must have a symmetric (antisymmetric) scat-

tering amplitude we can write

$$\begin{aligned} f_0 &= 2\lambda \sum_{\text{even } l} (2l+1) A_l P_l, \\ f_1 &= 2\lambda \sum_{\text{odd } l} (2l+1) A_l P_l, \\ f_2 &= 2\lambda \sum_{\text{even } l} (2l+1) A_l P_l, \end{aligned} \quad (\text{B2})$$

and, using Clebsch-Gordan coefficients we can write the particle scattering amplitudes in terms of the isospin amplitudes

$$\begin{aligned} f_{-+} &= \frac{1}{6}f_2 + \frac{1}{2}f_1 + \frac{1}{3}f_0, \\ f_{-0} &= \frac{1}{2}f_2 + \frac{1}{2}f_1, \end{aligned} \quad (\text{B3})$$

so that

$$\begin{aligned} f_{-+} &= \frac{1}{3}\lambda \sum_{\text{even } l} (2l+1)(A_l^2 + 2A_l P_l) \\ &\quad + \lambda \sum_{\text{odd } l} (2l+1) A_l P_l, \\ f_{-0} &= \lambda \sum_{\text{even } l} (2l+1) A_l P_l + \lambda \sum_{\text{odd } l} (2l+1) A_l P_l. \end{aligned} \quad (\text{B4})$$

Note that f_{-0} is just the original amplitude (B1) with even (odd) l waves identified with even (odd) isospin amplitudes.